

# Journal of Visualized Experiments

## Manganese oxide nanoparticle synthesis by thermal decomposition of manganese(II) acetylacetonate --Manuscript Draft--

<b>Article Type:</b>	Methods Article - JoVE Produced Video
<b>Manuscript Number:</b>	JoVE61572R1
<b>Full Title:</b>	Manganese oxide nanoparticle synthesis by thermal decomposition of manganese(II) acetylacetonate
<b>Section/Category:</b>	JoVE Bioengineering
<b>Keywords:</b>	nanoparticles; manganese(II) acetylacetonate; manganese oxide; oleylamine; dibenzyl ether; thermal decomposition; magnetic resonance imaging; x-ray diffraction; transmission electron microscopy; Fourier-transform infrared spectroscopy
<b>Corresponding Author:</b>	Margaret Bennewitz, Ph.D. West Virginia University Morgantown, WV UNITED STATES
<b>Corresponding Author's Institution:</b>	West Virginia University
<b>Corresponding Author E-Mail:</b>	margaret.bennewitz@mail.wvu.edu
<b>Order of Authors:</b>	Celia Martinez de la Torre Margaret Bennewitz, Ph.D.
<b>Additional Information:</b>	
<b>Question</b>	<b>Response</b>
Please indicate whether this article will be Standard Access or Open Access.	Standard Access (US\$2,400)
Please indicate the <b>city, state/province, and country</b> where this article will be <b>filmed</b> . Please do not use abbreviations.	Morgantown, West Virginia, United States

**TITLE:**

Manganese Oxide Nanoparticle Synthesis by Thermal Decomposition of Manganese(II) Acetylacetonate

**AUTHORS AND AFFILIATIONS:**

Celia Martinez de la Torre, Margaret F. Bennewitz

Department of Chemical and Biomedical Engineering, West Virginia University, Morgantown, WV, USA

Email address of co-author:

Celia Martinez de la Torre: (cemartinezdelatorre@mix.wvu.edu)

Corresponding author:

Margaret F. Bennewitz (margaret.bennewitz@mail.wvu.edu)

**KEYWORDS:**

nanoparticles, manganese(II) acetylacetonate, manganese oxide, oleylamine, dibenzyl ether, thermal decomposition, magnetic resonance imaging, x-ray diffraction, transmission electron microscopy, Fourier-transform infrared spectroscopy

**SUMMARY:**

This protocol details a facile, one-pot synthesis of manganese oxide (MnO) nanoparticles by thermal decomposition of manganese(II) acetylacetonate in the presence of oleylamine and dibenzyl ether. MnO nanoparticles have been utilized in diverse applications including magnetic resonance imaging, biosensing, catalysis, batteries, and waste water treatment.

**ABSTRACT:**

For biomedical applications, metal oxide nanoparticles such as iron oxide and manganese oxide (MnO), have been used as biosensors and contrast agents in magnetic resonance imaging (MRI). While iron oxide nanoparticles provide constant negative contrast on MRI over typical experimental timeframes, MnO generates switchable positive contrast on MRI through dissolution of MnO to  $\text{Mn}^{2+}$  at low pH within cell endosomes to 'turn ON' MRI contrast. This protocol describes a one-pot synthesis of MnO nanoparticles formed by thermal decomposition of manganese(II) acetylacetonate in oleylamine and dibenzyl ether. Although running the synthesis of MnO nanoparticles is simple, the initial experimental setup can be difficult to reproduce if detailed instructions are not provided. Thus, the glassware and tubing assembly is first thoroughly described to allow other investigators to easily reproduce the setup. The synthesis method incorporates a temperature controller to achieve automated and precise manipulation of the desired temperature profile, which will impact resulting nanoparticle size and chemistry. The thermal decomposition protocol can be readily adapted to generate other metal oxide nanoparticles (e.g., iron oxide) and to include alternative organic solvents and stabilizers (e.g., oleic acid). In addition, the ratio of organic solvent to stabilizer can be changed to further impact nanoparticle properties, which is shown herein. Synthesized MnO

nanoparticles are characterized for morphology, size, bulk composition, and surface composition through transmission electron microscopy, X-ray diffraction, and Fourier-transform infrared spectroscopy, respectively. The MnO nanoparticles synthesized by this method will be hydrophobic and must be further manipulated through ligand exchange, polymeric encapsulation, or lipid capping to incorporate hydrophilic groups for interaction with biological fluids and tissues.

## INTRODUCTION:

Metal oxide nanoparticles possess magnetic, electric, and catalytic properties, which have been applied in bioimaging<sup>1-3</sup>, sensor technologies<sup>4,5</sup>, catalysis<sup>6-8</sup>, energy storage<sup>9</sup>, and water purification<sup>10</sup>. Within the biomedical field, iron oxide nanoparticles and manganese oxide (MnO) nanoparticles have proven utility as contrast agents in magnetic resonance imaging (MRI)<sup>1,2</sup>. Iron oxide nanoparticles produce robust negative contrast on T<sub>2</sub>\* MRI and are powerful enough to visualize single labeled cells in vivo<sup>11-13</sup>; however, the negative MRI signal cannot be modulated and remains “ON” throughout the duration of typical experiments. Due to endogenous iron present in the liver, bone marrow, blood and spleen, the negative contrast generated from iron oxide nanoparticles may be difficult to interpret. MnO nanoparticles, on the other hand, are responsive to a drop in pH. MRI signal for MnO nanoparticles can transition from “OFF” to “ON” once the nanoparticles are internalized inside the low pH endosomes and lysosomes of the target cell such as a cancer cell<sup>14-19</sup>. The positive contrast on T<sub>1</sub> MRI produced from the dissolution of MnO to Mn<sup>2+</sup> at low pH is unmistakable and can improve cancer detection specificity by only lighting up at the target site within a malignant tumor. Control over nanoparticle size, morphology and composition is crucial to achieve maximum MRI signal from MnO nanoparticles. Herein, we describe how to synthesize and characterize MnO nanoparticles using the thermal decomposition method and note different strategies for fine-tuning nanoparticle properties by altering variables in the synthesis process. This protocol can be easily modified to produce other magnetic nanoparticles such as iron oxide nanoparticles.

MnO nanoparticles have been produced by a variety of techniques including thermal decomposition<sup>20-25</sup>, hydro/solvothermal<sup>26-29</sup>, exfoliation<sup>30-34</sup>, permanganates reduction<sup>35-38</sup>, and adsorption-oxidation<sup>39-42</sup>. Thermal decomposition is the most commonly used technique which involves dissolving manganese precursors, organic solvents, and stabilizing agents at high temperatures (180 – 360 °C) under the presence of an inert gaseous atmosphere to form MnO nanoparticles<sup>43</sup>. Out of all of these techniques, thermal decomposition is the superior method to generate a variety of MnO nanocrystals of pure phase (MnO, Mn<sub>3</sub>O<sub>4</sub> and Mn<sub>2</sub>O<sub>3</sub>) with a narrow size distribution. Its versatility is highlighted through the ability to tightly control nanoparticle size, morphology and composition by altering reaction time<sup>44-46</sup>, temperature<sup>44,47-49</sup>, and types/ratios of reactants<sup>20,45,47,48,50</sup> and inert gas<sup>47,48,50</sup> used. The main limitations of this method are the requirement for high temperatures, the oxygen-free atmosphere, and the hydrophobic coating of the synthesized nanoparticles, which requires further modification with polymers, lipids or other ligands to increase solubility for biological applications<sup>14,51-53</sup>.

Besides thermal decomposition, the hydro/solvothermal method is the only other technique that can produce a variety of MnO phases including MnO, Mn<sub>3</sub>O<sub>4</sub>, and MnO<sub>2</sub>; all other

strategies only form MnO<sub>2</sub> products. During hydro/solvothermal synthesis, precursors such as Mn(II) stearate<sup>54, 55</sup> and Mn(II) acetate<sup>27</sup> are heated to between 120-200 °C over several hours to achieve nanoparticles with a narrow size distribution; however, specialized reaction vessels are required and reactions are performed at high pressures. In contrast, the exfoliation strategy involves treatment of a layered or bulk material to promote dissociation into 2D single layers. Its main advantage is in producing MnO<sub>2</sub> nanosheets, but the synthesis process is long requiring several days and the resulting size of the sheets is difficult to control. Alternatively, permanganates such as KMnO<sub>4</sub> can react with reducing agents such as oleic acid<sup>56,57</sup>, graphene oxide<sup>58</sup> or poly(allylamine hydrochloride)<sup>59</sup> to create MnO<sub>2</sub> nanoparticles. Use of KMnO<sub>4</sub> facilitates nanoparticle formation at room temperature over a few minutes to hours within aqueous conditions<sup>43</sup>. Unfortunately, the rapid synthesis and nanoparticle growth makes it challenging to finely control resulting nanoparticle size. MnO<sub>2</sub> nanoparticles can also be synthesized using adsorption-oxidation whereby Mn<sup>2+</sup> ions are adsorbed and oxidized to MnO<sub>2</sub> by oxygen under basic conditions. This method will produce small MnO<sub>2</sub> nanoparticles with a narrow size distribution at room temperature over several hours in aqueous media; however the requirement for adsorption of Mn<sup>2+</sup> ions and alkali conditions limits its widespread application<sup>43</sup>.

Of the MnO nanoparticle synthesis methods discussed, thermal decomposition is the most versatile to generate different monodisperse pure phase nanocrystals with control over nanoparticle size, shape and composition without requiring specialized synthesis vessels. In this manuscript, we describe how to synthesize MnO nanoparticles by thermal decomposition at 280°C using manganese(II) acetylacetonate (Mn(II)ACAC) as the source of Mn<sup>2+</sup> ions, oleylamine (OA) as the reducing agent and stabilizer, and dibenzyl ether (DE) as the solvent under a nitrogen atmosphere. The glassware and tubing setup for nanoparticle synthesis is explained in detail. One advantage of the technique is the inclusion of a temperature controller, thermocouple probe, and heating mantle to enable precise control over the heating rate, peak temperature, and reaction times at each temperature to fine-tune nanoparticle size and composition. Herein, we show how nanoparticle size can also be manipulated by changing the ratio of OA to DE. Additionally, we demonstrate how to prepare nanoparticle samples and measure nanoparticle size, bulk composition and surface composition using transmission electron microscopy (TEM), x-ray diffraction (XRD), and Fourier-transform infrared spectroscopy (FTIR), respectively. Further guidance is included on how to analyze the collected images and spectra from each instrument. To generate uniformly shaped MnO nanoparticles, a stabilizer and adequate nitrogen flow must be present; XRD and TEM results are shown for undesired products formed in the absence of OA and under low nitrogen flow. In the Discussion section, we highlight crucial steps in the protocol, metrics to determine successful nanoparticle synthesis, further variation of the decomposition protocol to modify nanoparticle properties (size, morphology and composition), troubleshooting and limitations of the method, and applications of MnO nanoparticles as contrast agents for biomedical imaging.

## **PROTOCOL:**

### **1. Glassware and tubing assembly – to be performed only the first time**

NOTE: **Figure 1** shows the experimental setup for MnO nanoparticle synthesis with numbered tubing connections. **Figure S1** shows the same setup with the main glassware components labeled. If there is a mismatch between the chemical resistant tubing and the glass connection size, cover the glass connection first with a short piece of smaller tubing before adding the chemical resistant tubing to make the connections snug.

1.1. Secure the air-free nitrogen tank to the wall close to a chemical fume hood using approved strap restraints. Add the appropriate nitrogen regulator to the tank.

CAUTION: Gas cylinders must be properly secured since they can be very dangerous if tipped over.

1.2. Fill the gas drying column with desiccant. Attach chemical resistant tubing from the air-free nitrogen regulator to the bottom inlet of the gas drying column (#1 in **Figure 1**).

1.3. Secure the glass manifold containing at least 2 outlet stopcocks to the top of the fume hood using two metal claw clamps. Attach chemical resistant tubing from the outlet of the gas drying column (#2 in **Figure 1**) to the inlet of the manifold (#3 in **Figure 1**).

1.4. Place and secure 3 mineral oil bubblers in the fume hood using metal claw clamps according to **Figure 1**. Put two bubblers to the left and one bubbler to the right.

1.5. Fill the leftmost bubbler (by #9 in **Figure 1**) with the smallest amount of silicone oil (~1 inch of oil from the bottom of the bubbler). Fill the middle bubbler (by #7,8 in **Figure 1**) with a medium amount of silicone oil (~1.5 inches of oil from the bottom of the bubbler). Fill the rightmost bubbler (by #11 in **Figure 1**) with the largest amount of silicone oil (~2 inches of oil from the bottom of the bubbler).

NOTE: The relative amount of silicone oil between the mineral bubblers is very important to achieve appropriate flow of the air-free nitrogen gas through the system. Do not add too much oil (over ~2.5 inches), as the oil will bubble during the reaction and can exit the bubblers if overfilled.

1.6. Connect the outlet on the right stopcock of the manifold (#4 in **Figure 1**) to the threaded end of a glass elbow adapter (#5 in **Figure 1**) using chemical resistant tubing.

1.7. Attach the threaded end of another glass elbow adapter (#6 in **Figure 1**) to the inlet of the middle bubbler (#7 in **Figure 1**) using chemical resistant tubing. Connect the outlet of the middle bubbler (#8 in **Figure 1**) to the inlet of the leftmost bubbler (#9 in **Figure 1**) using chemical resistant tubing.

1.8. Connect the outlet on the left stopcock of the manifold (#10 in **Figure 1**) to the inlet of the rightmost bubbler (#11 in **Figure 1**).

1.9. Leave the preliminary setup in the fume hood if space accommodates. Secure the two glass elbow adapters with tubing attached (#5,6 in **Figure 1**) to the metal latticework in the fume hood when the experiment is not running.

## 2. **Equipment and glassware setup – to be performed during every experiment**

CAUTION: All steps involving solvents require the use of a chemical fume hood as well as proper personal protective equipment (PPE) including safety glasses, lab coat and gloves. The nanoparticle fabrication setup should be assembled in the fume hood.

2.1. Place the stir plate in the fume hood and put the heating mantle on top of the stir plate.

NOTE: The heating mantle must be able to withstand temperatures above 300 °C.

2.2. Put the 4 neck 500 mL round bottom flask onto the heating mantle and secure the middle neck with a metal claw clamp. Add a magnetic stir bar to the round bottom flask. Place the glass funnel in the middle neck of the round bottom flask.

2.3. Check the manifold: make sure the safety stopcock (#10 in **Figure 1**) and input stopcock (#4 in **Figure 1**) are open.

CAUTION: The safety stopcock needs to be open at all times to assure no pressure is built up in the system. If the stopcock is closed, an explosion can occur.

2.4. Weigh 1.51 g of manganese(II) acetylacetonate (Mn(II) ACAC) and place inside the round bottom flask using the glass funnel.

2.5. Add 20 mL of oleylamine and 40 mL of dibenzyl ether to the round bottom flask using a glass pipette and the glass funnel. Remove the funnel and clean it with hexane.

CAUTION: The experiment can be scaled up (e.g., 2 times), but it is recommended to be conservative when using any larger quantities of reactants. Larger amounts of reactants could cause the reaction to become less stable, and therefore dangerous.

2.6. Attach the condenser to the left neck of the round bottom flask and secure the condenser with a metal claw clamp. Add the glass elbow adapter (#6 in **Figure 1**) on top of the condenser.

NOTE: The adapter should be connected with chemical resistant tubing to the middle mineral oil bubbler (#7 in **Figure 1**).

2.7. Connect water compatible tubing from the water outlet spout in the fume hood (#12 in **Figure 1**) to the inlet of the condenser (#13 in **Figure 1**). Also use water compatible tubing to

connect the outlet of the condenser (#14 in **Figure 1**) to the drain in the fume hood (#15 in **Figure 1**). Secure the tubing to the condenser connections (#13,14 in **Figure 1**) with interlocked worm gear metal hose clamps.

2.8. Add the rotovap trap to the right neck of the round bottom flask. Place the glass elbow adapter (#5 in **Figure 1**) on top of the rotovap trap.

NOTE: The adapter should be connected with chemical resistant tubing to the right stopcock manifold outlet (#4 in **Figure 1**).

2.9. Attach the rubber stopper to the middle neck of the round bottom flask and fold it over so the sides cover the neck of the flask. Add the plastic conical joint clips (4 green clips in **Figure 1**) to secure the following glassware neck connections: elbow adapter and rotovap trap, rotovap trap and round bottom flask, round bottom flask and condenser, and condenser and elbow adapter.

2.10. Place the temperature probe into the smallest neck in the round bottom flask, tightening and securing the probe with the neck cap and the o-ring. Seal the connection with paraffin plastic film.

NOTE: Make sure the temperature probe is immersed within the fluid mixture, but does not touch the bottom of the glass. If the probe is in contact with the glass surface, the temperature measured will be inaccurate compared to the true fluid temperature, which will cause the temperature controller to provide an incorrect amount of heat to the reaction.

2.11. Connect the temperature probe to the input of the temperature controller. Connect the heating mantle to the output of the temperature controller.

2.12. Turn on the stir plate and start stirring vigorously.

2.13. Open the air-free nitrogen tank and slowly begin flowing nitrogen into the system (this will remove the air). Adjust the nitrogen flow using the regulator until a steady slow stream of bubbles form in the middle mineral oil bubbler (#7 in **Figure 1**).

2.14. Turn on the cold water in the fume hood (#12 in **Figure 1**) to the condenser and check that no water leaks from the tubing.

2.15. Put the sash of the fume hood down before the reaction begins.

### 3. Nanoparticle synthesis

3.1. Turn on the temperature controller (power and heating supply) to start the reaction. Observe and record the color of the reaction mixture in each stage. The reaction will begin as a dark brown color in stages 1 to 3 and will turn green during stage 4.

NOTE: Each temperature controller will work differently. Make sure to use the correct manual and program.

3.2. Stage 1: Observe the temperature controller display to confirm the temperature increases from room temperature to 60 °C over 30 min.

3.3. Stage 2: Ensure that the temperature controller stabilizes at 60 °C for 1 min as it prepares for a faster heating rate in stage 3.

3.4. Stage 3: Check the temperature controller display as the temperature rises to 280 °C at 10 °C per minute over 22 min. Make sure the water flow through the condenser is sufficient, as the mixture will start to evaporate during this stage.

3.5. Stage 4: Confirm the temperature controller displays a constant reaction temperature of 280 °C for 30 min. Observe the reaction color change to a green tone, which indicates MnO formation. Once the reaction reaches 280 °C, turn off the nitrogen tank and close the right stopcock for the inlet of the reaction on the manifold (#4 in **Figure 1**).

CAUTION: Keep the safety stopcock (#10 in **Figure 1**) open.

3.6. Stage 5: Check the temperature controller display to ensure that the heating stops automatically. Keep the temperature probe inside (do not open the round bottom flask) and wait until the temperature reaches room temperature to proceed with nanoparticle collection.

CAUTION: The flask will be extremely hot. Heat resistant gloves should be worn to remove the heating mantle if a faster cooling rate is desired.

NOTE: The protocol can be paused here.

#### 4. Nanoparticle collection

4.1. Turn off the temperature controller, the stir plate and the cold water. Remove the water compatible tubing from the condenser, water faucet in the fume hood and the drain. Remove all the plastic conical joint clips from glassware connections.

4.2. Remove the glass elbow adapters from the rotovap trap (#5 in **Figure 1**) and the condenser (#6 in **Figure 1**). Secure the elbow adapters to the metal latticework in the hood to use for a future experiment.

4.3. Detach the condenser and rotovap trap from the round bottom flask and rinse the insides of the condenser and rotovap trap with hexane.

4.4. Remove the rubber stopper and temperature probe, and clean with 70% ethanol.



4.5. Pour the MnO nanoparticle solution from the round bottom flask into a clean 500 mL beaker. Use hexane (~5 mL) to rinse the round bottom flask and add the hexane with residual MnO nanoparticles into the 500 mL beaker.

NOTE: Hexane will resuspend the MnO nanoparticles while 200 proof ethanol will act as the precipitant agent.

4.6. Note the current volume of the MnO nanoparticle mixture. Add 200 proof ethanol to the MnO nanoparticle mixture using a volume ratio of 2:1 (e.g., add 150 mL of ethanol if the nanoparticle mixture is 75 mL).

4.7. Pour the nanoparticle mixture equally into four centrifuge tubes, around 3/4 full. Screw on the appropriate caps. Check to make sure the fluid levels are balanced.

NOTE: Any extra nanoparticle mixture will be added to the tubes on the next round of centrifugation.

4.8. Centrifuge nanoparticles for 10 min at 17,400 x *g* at 10 °C.

NOTE: Longer centrifugation times and/or higher centrifugation speeds can be used to increase collection of smaller nanoparticle fractions, but nanoparticle aggregation can be increased.

4.9. Discard the supernatant into a waste beaker, being careful not to disturb the pellet. If needed, use a transfer pipette to collect the supernatant.

NOTE: It is normal for the early rounds of centrifugation to produce a brown colored supernatant. The supernatant should be brown and clear, but not cloudy. Any cloudiness indicates that the nanoparticles are still present in the supernatant. If the supernatant is cloudy, centrifuge the tubes again before discarding the supernatant; centrifuging again will reduce loss of the synthesized nanoparticles, but can cause more agglomeration.

4.10. Add 5 mL of hexane and any extra nanoparticle solution left to each centrifuge tube containing the MnO nanoparticle pellets. Resuspend the nanoparticles using a bath sonicator and/or vortex. Continue until the solution becomes cloudy and the pellet disappears, which indicates successful nanoparticle resuspension.

4.11. Add more 200 proof ethanol to the centrifuge tubes until 3/4 full.

4.12. Repeat steps 4.8-4.10. Then, combine the resuspended nanoparticles from four centrifuge tubes to two centrifuge tubes. Next, repeat step 4.11.

4.13. Repeat steps 4.8-4.10 once more, which will make a total of three washes with hexane and 200 proof ethanol. Do not add any 200 proof ethanol to the centrifuge tubes.

4.14. Combine and transfer the MnO nanoparticles resuspended in hexane into a preweighed 10 mL glass scintillation vial. Leave the lid of the vial off to allow the hexane to evaporate overnight in the fume hood.

4.15. The next day, transfer the uncovered glass scintillation vial containing the nanoparticles into a vacuum oven. Keep the lid for the vial in a safe place outside the oven. Dry out the nanoparticles at 100°C for 24 hours.

4.16. Once nanoparticles are dried, use a spatula to break up the powder inside the vial. Weigh the vial containing dried MnO nanoparticles and subtract the known weight of the glass scintillation vial to determine the nanoparticle yield.

CAUTION: Dried nanoparticles can easily become airborne and should be handled by personnel using a particle respirator such as N95 or P100.

4.17. Store nanoparticles at room temperature inside the glass scintillation vial with the lid on. Wrap the lid with paraffin plastic film.

## 5. Nanoparticle size and surface morphology (TEM)

5.1. Pulverize the MnO nanoparticles into a thin powder using a mortar and pestle.

5.2. Add 5 mg of MnO nanoparticles to a 15 mL conical centrifuge tube. Add 10 mL of 200 proof ethanol.

NOTE: 200 proof ethanol evaporates quickly to obtain a more homogeneous spread of nanoparticles on the TEM grid. Another solvent could have better nanoparticle suspension, but would take longer to evaporate, and due to surface tension, the nanoparticles would accumulate on the borders of the TEM grids.

5.3. Bath sonicate the nanoparticle mixture for 5 min or until full resuspension of the nanoparticles.

5.4. Immediately upon resuspension, add three 5 µL drops of the nanoparticle mixture onto a 300 mesh copper grid support film of carbon type-B. Let air dry.

5.4.1. Use reverse tweezers for easier sample preparation. Position the grid on the tweezers with the darker side up before adding the drops containing nanoparticles.

NOTE: The grids are fragile, so be careful not to bend and damage the grids for better imaging. Once dry, grids should be kept inside commercially available TEM grid storage boxes for protection.

5.5. Assess nanoparticle shape and size using transmission electron microscopy (TEM). Apply typical parameters for TEM including a beam strength of 200 kV, a spot size of 1, and a magnification of 300x.

5.6. Collect images on areas of the grid where enough nanoparticles (10 - 30 nanoparticles) are evenly distributed. Avoid areas containing nanoparticle aggregations, as accurate sizing cannot be made if nanoparticles are not visibly separated.

5.6.1. Image areas from different grid squares to assure an even distribution. For an optimal size distribution, take between 25 - 30 images from each sample to obtain a sufficient sample size.

## 6. Quantitative analysis of nanoparticle diameter

6.1. To analyze TEM images with ImageJ, first open one of the images by clicking **File | Open**. Select the desired image and click **Open**.

6.2. To calibrate the distance measurement in ImageJ from pixels to nanometers, first click the straight-line tool. Hold the **Shift** key and trace the length of the scale bar. Then, click **Analyze | Set Scale**.

6.3. In the Set Scale pop-up window, type the true scale bar measurement into the **Known distance** box (e.g., type 50 if the scale bar is 50 nm). Change the unit of length to the corresponding units (e.g., type nm for nanometers). Check the **Global** box to keep the scale consistent in all the images, and click **OK**.

6.4. After setting the scale, use the straight-line tool to trace the diameter of a nanoparticle. Then click **Analyze | Measure** or click **Ctrl+M** keys.

6.5. Look for a results pop-up window to appear with different information about the measurement. Confirm that the "Length" column is present, as it will provide the diameter of the nanoparticles with the units specified during step 6.3.

6.6. Repeat step 6.4 until all the nanoparticles in the image are sized. To move to the next image, either click **File | Open Next**, or **Ctrl+Shift+O** keys.

6.7. After all nanoparticles are sized in all images, go to the **Results** window and click **File | Save As**. Rename the results file and click **Save**. View and analyze all nanoparticle diameters in a spreadsheet program after importing the results file.

## 7. Nanoparticle bulk composition (XRD)

7.1. If not done during step 5.1, pulverize the MnO nanoparticles into a thin powder using a mortar and pestle. Place the fine nanoparticle powder into the sample holder using a spatula.

Follow the sample loading procedure specified for the X-ray diffraction (XRD) machine to be used.

7.2. Determine bulk composition of MnO nanoparticles using XRD. Collect XRD spectra over a  $2\theta$  range from  $10^\circ$  to  $110^\circ$  to view peaks of MnO ( $30^\circ$  to  $90^\circ$ ) and  $\text{Mn}_3\text{O}_4$  ( $15^\circ$  to  $90^\circ$ ).

NOTE: Other setting parameters recommended for XRD are a step size of 0.05 s, a beam mask of 10 mm, and a scan step time of 64.77 s.

7.3. Save the generated .XRD file and open it in the XRD analysis program.

## 8. Analysis of XRD spectra

8.1. In the XRD analysis program, identify all the main peaks in the sample's measured XRD spectrum by clicking on the **IdeAll** button in the software.


8.2. To save the data, select **File** on the toolbar, followed by **Save as...** to save the data as an ASC file that can be opened with a spreadsheet program.

8.3. Use the program to pattern match the XRD database of known compounds to find the best composition match to the sample. To narrow the search, specify anticipated compounds (e.g., manganese and oxygen).

8.3.1. To pattern match the spectrum, select "**Analysis | Search & Match**". In the pop-up window, select **Chemistry** and click the desired chemical elements to restrict the program search based on the sample.

8.3.2. Once all elements are chosen, select **Search**. Wait for a list of chemical compositions matching the XRD spectrum to appear.

NOTE: The program will provide the likelihood that known XRD spectra correspond to the sample's composition. If two or more compositions are chosen, the program would give the composition percentage of each of them (e.g., MnO versus  $\text{Mn}_3\text{O}_4$ ).

8.4. If desired, remove the background from the XRD spectrum by clicking the **Fit Background** button (  ). Then, click **Background** in the pop-up window, followed by **Subtract**. Confirm that the spectrum appears starting with 0 on the y-axis.

8.4.1. Save the data again without the background as shown in step 8.2.

8.5. When plotting the XRD spectrum, show the characteristic peaks of each matched compound (e.g., MnO and  $\text{Mn}_3\text{O}_4$ ).

8.5.1. To obtain the list of the characteristic peaks for matched compounds from the database, first right click on the pattern match spectrum, and then select “Show Pattern”. Wait for a pop-up window to appear with all the peak information corresponding to the selected pattern.

8.5.2. Select, copy and paste the desired information from that compound and plot the characteristic peaks with the measured XRD spectrum in a spreadsheet program.

## 9. Nanoparticle surface composition (FTIR)

9.1. Add dry MnO nanoparticle powder to the sample holder for Fourier-transform infrared spectroscopy (FTIR) analysis.

9.2. Evaluate nanoparticle surface chemistry using FTIR. Collect FTIR spectra between a 4000 and 400  $\text{cm}^{-1}$  wavelength range with a resolution of 4  $\text{cm}^{-1}$ .

9.3. Clean the FTIR sample holder and add liquid oleylamine. Repeat Step 9.2.

## 10. Analysis of FTIR spectra

10.1. In the FTIR analysis program, remove the background from the collected FTIR spectrum by selecting **Transforms** in the drop-down menu, followed by **Baseline Correct**. Select **Linear** as the correction type.

10.2. Use the left mouse click to select the baseline points on the original spectrum. Once finished, save the spectrum under another name by selecting **Add** or replace the old spectrum by selecting **Replace**.

NOTE: Background correction can enhance the prevalence of weaker FTIR peaks of interest.

10.3. To export the FTIR spectrum, first select the specific spectrum from the list. Then, click **File** on the toolbar, followed by **Export spectrum**.

10.4. Choose csv file format from the **Save As** window and click **Save**. Open and graph the csv file using a spreadsheet program.

10.5. Compare acquired MnO nanoparticle with oleylamine FTIR spectra as detailed in the Representative Results section to evaluate nanoparticle capping with oleylamine.

## REPRESENTATIVE RESULTS:

To confirm successful synthesis, MnO nanoparticles should be assayed for size and morphology (TEM), bulk composition (XRD), and surface composition (FTIR). **Figure 2** shows representative TEM images of MnO nanoparticles synthesized using decreasing ratios of oleylamine (OA, the stabilizer) to dibenzyl ether (DE, the organic solvent): 60:0, 50:10, 40:20, 30:30, 20:40, 10:50.

Ideal TEM images consist of individual nanoparticles (shown as dark rounded octagons in **Figure 2**), with minimal overlap. It is crucial to achieve adequate separation of nanoparticles for accurate manual sizing of the nanoparticle diameters using the line trace tool in ImageJ.

**Figure 3** shows suboptimal TEM sample preparation. If a high concentration of MnO nanoparticles are suspended in ethanol or too many drops of nanoparticle suspension are added to the TEM grid, each image will consist of large agglomerations of nanoparticles (**Figure 3A,B**). Due to the substantial overlap of nanoparticles, the limits of each nanoparticle diameter cannot be distinguished, which prevents accurate measurement. If a low nanoparticle concentration is prepared in ethanol, nanoparticles could be well separated, but distributed sparsely on the TEM grid (**Figure 3C,D**). When only one or two nanoparticles appear in each TEM image, more images need to be taken to gain a large enough sample size and the full size distribution may not be precisely captured. The TEM preparation protocol described herein aims to produce TEM images with approximately 10-30 nanoparticles per image (more nanoparticles can be accommodated per image if the diameter is small).

TEM can be used to evaluate changes in nanoparticle size with a variation in synthesis parameters. **Figure 4** shows the average diameters of MnO nanoparticles synthesized with decreasing ratios of OA:DE. Diameters for each synthesis condition were quantified from 75 to 90 TEM images, with a total of 900 to 1100 MnO nanoparticles analyzed per condition. To ensure reproducibility, 3 batches of nanoparticles were synthesized for each OA:DE ratio. Overall, a decrease in the ratio of OA:DE yielded smaller MnO nanoparticles with less variation in size; the only exception occurred when OA alone was used during synthesis, which produced similar sized nanoparticles to the 30:30 ratio. Histograms showing the full size distribution of all MnO nanoparticle groups are displayed in **Figure S2**.

After confirming nanoparticle size and morphology with TEM, the bulk nanoparticle composition can be tested using XRD. Through measuring the angle and intensity of the X-ray beam diffracted by the sample, XRD can be used to determine crystal structure and phase of the nanoparticles. **Figure 5A-F** shows the raw collected XRD spectra for each synthesized MnO nanoparticle sample with decreasing ratios of OA:DE. The XRD peaks obtained on sample spectra are matched to XRD peaks from known compounds such as MnO and Mn<sub>3</sub>O<sub>4</sub> through the XRD analysis program database. The standard peaks for MnO appear at 35°, 40°, 58°, 70°, 73°, and 87°, which are shown in **Figure 5G**. When comparing the nanoparticle XRD spectra with known MnO, it is evident that all nanoparticle spectra possess the 5 highest peaks of MnO, indicating successful synthesis of MnO nanoparticles. XRD can also be utilized to estimate nanoparticle size using the Scherrer equation; wider peaks on XRD indicate smaller nanoparticle diameters. For example, **Figure 5F** with the widest XRD peaks is associated with the smallest nanoparticles as shown by TEM ( $18.6 \pm 5.5$  nm).

**Figure 6** shows XRD spectra of two undesired products in MnO nanoparticle synthesis. To encourage the formation of the MnO phase at high temperatures (280°C), nitrogen is used during nanoparticle synthesis to purge air out of the system. If inadequate nitrogen flow is applied, a mixed phase composition of Mn<sub>3</sub>O<sub>4</sub> (51%) and MnO (49%) is produced (**Figure 6A**).

Through comparison with the standard peaks of  $\text{Mn}_3\text{O}_4$  (**Figure 6C**) and  $\text{MnO}$  (**Figure 6D**), low nitrogen flow produces XRD spectra with the 8 highest peaks for  $\text{Mn}_3\text{O}_4$  and the 5 highest peaks for  $\text{MnO}$ . TEM of nanoparticles synthesized under low nitrogen flow revealed a mixed population of large nanoparticles surrounded by smaller nanoparticles (**Figure 6E**). Nitrogen flow can be monitored through the nitrogen regulator reading and the rate of bubbling through the mineral oil bubbler. Another critical parameter in  $\text{MnO}$  nanoparticle synthesis is the inclusion of a stabilizer. In an attempt to produce even smaller  $\text{MnO}$  nanoparticles than the 10:50 OA:DE ratio, pure DE was used without any OA. A very small amount of an unknown powder was synthesized in the absence of stabilizer. As shown in **Figure 6B**, the XRD spectra for the 0:60 OA:DE ratio was noisy and contained the 3 highest peaks of  $\text{Mn}_3\text{O}_4$ . From analysis in the XRD program database, the compound had a chemical composition of 67%  $\text{Mn}_3\text{O}_4$  and 33%  $\text{MnO}$ . As supported by the wide peaks in the XRD spectra, the TEM confirmed that very small nanoparticles were synthesized in the absence of stabilizer (**Figure 6F**). Nanoparticles also appeared irregularly shaped and agglomerated. Additionally, only a 33% yield was obtained without any stabilizer, meaning that a small amount of product was synthesized. Therefore, high nitrogen flow and inclusion of a stabilizer such as OA or oleic acid is necessary for synthesis of  $\text{MnO}$  nanoparticles.

To complement bulk nanoparticle composition with XRD, surface composition can be evaluated using FTIR. **Figure 7** shows the FTIR spectra of  $\text{MnO}$  nanoparticles after background correction. All spectra show the symmetric and asymmetric  $\text{CH}_2$  peaks ( $2850\text{--}2854$  and  $2918\text{--}2926\text{ cm}^{-1}$ , marked by asterisks) associated with oleyl groups<sup>60</sup>, in addition to the  $\text{NH}_2$  bending vibration peaks ( $1593\text{ cm}^{-1}$  and  $3300\text{ cm}^{-1}$ , marked by squares) associated with amine groups<sup>61</sup>. Since  $\text{MnO}$  nanoparticles share the same peaks for oleyl groups and amine groups present in the FTIR spectra of OA (**Figure S3**), it can be concluded that the nanoparticles are coated with a surface layer of OA. Furthermore, all nanoparticle FTIR spectra contain Mn-O and Mn-O-Mn bond vibrations around  $600\text{ cm}^{-1}$  (marked by triangles), which confirm the composition found through XRD<sup>62</sup>.

#### FIGURE LEGENDS:

**Figure 1: Nitrogen and water flow through the  $\text{MnO}$  nanoparticle synthesis setup.** Tubing connections are labeled 1-15. Air-free nitrogen enters (1) and exits (2) the drying column and is fed into the inlet of the manifold (3). During the reaction, nitrogen purges air from the system by entering the right stopcock on the manifold (4). Nitrogen flows from the stopcock to the glass elbow adapter (5), rotovap trap, round bottom flask, condenser, glass elbow adapter (6) and through a series of two mineral oil bubblers (7-9). In the manifold, excess nitrogen not flowing through the reaction will leave the system through the left stopcock (10), which is connected to the mineral oil bubbler with the largest amount of silicone oil (11). Stopcock #10 is to always remain open. Water will flow from the faucet (12) through the condenser inlet (13) and outlet (14) and into the fume hood drain (15). The tubing is secured to the condenser with metal clamps. All tubing should be chemical resistant tubing except for the water compatible tubing used for the condenser. The main glassware and equipment are labeled in **Figure S1**.

**Figure 2: TEM images of MnO nanoparticles synthesized with decreasing ratios of OA:DE.** The following ratios were used: (A) 60:0, (B) 50:10, (C) 40:20, (D) 30:30, (E) 20:40, (F) 10:50. MnO nanoparticles appear as separate, rounded octagons with minimal overlap to allow for clear delineation of nanoparticle borders. The reactant ratio was observed to affect overall nanoparticle size, with 50:10 synthesizing the largest nanoparticles and 10:50 producing the smallest nanoparticles. Scale bars are 50 nm.

**Figure 3: Suboptimal TEM images resulting from incorrect TEM grid preparation.** (A,B) If the nanoparticle suspension is too concentrated or if excess drops of nanoparticle suspension get loaded onto the TEM grid, nanoparticles will aggregate into large masses with substantial overlap. Individual nanoparticles cannot be observed in most areas of the grid. (C,D) Alternatively, a low nanoparticle concentration could result in TEM grids populated with a scarce amount of nanoparticles. Individual nanoparticles are spread far apart, but require more images to capture the sample's population size distribution. Scale bars are 50 nm.

**Figure 4: Average MnO nanoparticle diameters measured from TEM images.** In general, a lower amount of stabilizer (OA) with a higher amount of organic solvent (DE) resulted in smaller, more uniform MnO nanoparticles. A total of 900 to 1100 nanoparticle diameters were calculated on TEM images using the line trace tool in ImageJ for each group. Error bars show standard deviation.

**Figure 5: XRD spectra of MnO nanoparticles synthesized with decreasing ratios of OA:DE.** The following ratios were used: (A) 60:0, (B) 50:10, (C) 40:20, (D) 30:30, (E) 20:40, (F) 10:50. (G) The standard diffraction peaks for MnO are shown from the XRD analysis program database. All nanoparticles produced exhibit the 5 highest intensity XRD peaks for MnO, indicating successful synthesis of MnO nanoparticles.

**Figure 6: XRD spectra and TEM images of undesired nanoparticles.** XRD spectra are shown for MnO nanoparticle synthesis using (A) low nitrogen flow and (B) a 0:60 ratio of OA:DE (no stabilizer is present). The standard diffraction peaks for (C)  $\text{Mn}_3\text{O}_4$  and (D) MnO are displayed from the XRD analysis program database. Through comparison with standard spectra, inadequate nitrogen flow (A) created nanoparticles with a mixture of  $\text{Mn}_3\text{O}_4$  (51%) and MnO (49%). In the absence of oleylamine (B), a broader XRD spectrum is obtained, which matches the 3 highest peaks of  $\text{Mn}_3\text{O}_4$ . Based on the analysis performed by the XRD program database, these synthesized nanoparticles are 67%  $\text{Mn}_3\text{O}_4$  and 33% MnO. TEM images of (E) nanoparticles synthesized with low nitrogen flow show large nanoparticles surrounded by smaller ones. TEM images of (F) nanoparticles synthesized with a 0:60 ratio of OA:DE display very small aggregated nanoparticles with irregular shape. Scale bars are 50 nm.

**Figure 7: FTIR spectra of MnO nanoparticles synthesized with decreasing ratios of OA:DE.** The following ratios were used: (A) 60:0, (B) 50:10, (C) 40:20, (D) 30:30, (E) 20:40, (F) 10:50. Asterisks and squares correspond to oleyl groups and amine groups, respectively, while triangles indicate the vibration of Mn-O and Mn-O-Mn bonds. The boxed insets highlight the two distinct peaks of oleyl groups. FTIR spectra indicate that MnO nanoparticles are coated



with oleylamine, as confirmed through comparison with the oleylamine only FTIR spectrum in Figure S3.

**Figure S1: Major glassware and equipment of the MnO nanoparticle synthesis setup.** The manifold is secured to the metal lattice by metal claw clamps and disperses nitrogen into the reaction. Mn(II) ACAC, dibenzyl ether, oleylamine and a stir bar are added to the round bottom flask with four necks. The right neck of the flask is attached to the rotovap trap and an elbow adapter, while the left neck is attached to a condenser and an elbow adapter. The middle neck of the round bottom flask is covered with a rubber stopper. The temperature probe is inserted into the smallest opening of the round bottom flask, and is surrounded by an o-ring and paraffin plastic film to form an air-tight seal. The round bottom flask sits on top of a heating mantle and a stir plate to vigorously stir the reaction while heating. The temperature probe and heating mantle are connected to the temperature controller to provide real-time automated regulation of the temperature profile. The round bottom flask and condenser are secured to the metal lattice with metal claw clamps. There are three mineral oil bubblers, two on the left and one on the right, filled with increasing amounts of silicone oil from the left bubbler to right bubbler in the image. The bubblers are also attached to the metal lattice with claw clamps. Green plastic conical joint clips are attached to secure glassware connections before the reaction begins. The tubing connections are detailed in **Figure 1**.

**Figure S2: Histograms showing distribution of MnO nanoparticle size for decreasing ratios of OA:DE.** The following ratios were used: (A) 60:0, (B) 50:10, (C) 40:20, (D) 30:30, (E) 20:40, (F) 10:50. Overall as the ratio approaches 10:50, the nanoparticle size distribution shifts to the left (indicating smaller diameters) and becomes more compact (indicating more uniform nanoparticle size). The average diameter for each distribution is shown in **Figure 4**.

**Figure S3: FTIR spectrum of oleylamine.** Asterisks and squares represent the oleyl groups and amine groups of oleylamine, respectively.

## DISCUSSION:

The protocol herein describes a facile, one-pot synthesis of MnO nanoparticles using Mn(II) ACAC, DE, and OA. Mn(II) ACAC is utilized as the starting material to provide a source of  $\text{Mn}^{2+}$  for MnO nanoparticle formation. The starting material can be easily substituted to enable production of other metal oxide nanoparticles. For example, when iron(III) ACAC is applied,  $\text{Fe}_3\text{O}_4$  nanoparticles can be generated using the same nanoparticle synthesis equipment and protocol described<sup>63</sup>. DE serves as an ideal organic solvent for thermal decomposition reactions, as it has a high boiling point of 295-298 °C. OA is a commonly used inexpensive stabilizer/mild reducing agent, which aids in capping and coordinating metal oxide nanoparticle nucleation and growth<sup>61,63</sup>. Similar to DE, OA has a high boiling point of 350 °C to withstand the high temperatures of thermal decomposition. The following two observations can be used as evidence of successful generation of MnO nanoparticles during synthesis: 1) the appearance of a green hue to the reaction mixture during thermal decomposition at 280 °C and 2) the formation of a dark brown large pellet on the bottom of the centrifuge tubes following centrifugation in hexane and ethanol. Resulting nanoparticles should be further characterized

by TEM, XRD and FTIR to evaluate size/morphology, bulk composition and surface composition, respectively.

During nanoparticle synthesis, several variables must be noted and controlled to ensure production of uniform nanoparticles with the MnO crystalline phase. First, the ratio of all starting materials should remain the same, as we have shown that decreasing ratios of OA to DE decrease nanoparticle size (**Figure 4**). Second, the reaction should be vigorously stirred to enable adequate dispersion of nucleating nanoparticles, uniform heating, and reduction of size variation. Third, as temperature plays a large role in controlling metal oxide nanoparticle size<sup>47,48,50</sup> and phase composition<sup>47,48,50</sup>, it is critical to properly immerse the temperature probe tip into the reaction mixture while not contacting the glass of the round bottom flask that will read an inaccurate temperature. Fourth, the flow of nitrogen should be high enough to purge all air from the reaction to encourage formation of the MnO crystalline phase over Mn<sub>3</sub>O<sub>4</sub>. As shown in **Figure 6A**, low nitrogen flow will result in nanoparticles with a mixed MnO/Mn<sub>3</sub>O<sub>4</sub> composition. Correct filling of the mineral oil bubblers with increasing amounts of silicone oil from the left bubbler (1 inch of oil) to the middle bubbler (1.5 inches of oil) to the right bubbler (2 inches of oil) will set the resistance for nitrogen flow to be lowest through the reaction (#4 in **Figure 1**). The bubbling rate of the middle mineral oil bubbler (by #7,8 in **Figure 1**) can be used to measure the rate of nitrogen flowing through the reaction. Finally, a stabilizer such as OA must be added to the reaction mixture to coordinate nanoparticle nucleation and growth. As shown in **Figure 6B**, DE without OA created a small amount of product, mostly of a Mn<sub>3</sub>O<sub>4</sub> (67%) composition. This product was also observed to have an irregular shape with aggregated nanoparticles by TEM, which did not occur when OA was present in the reaction (**Figure 6F**).

Several variables of the thermal decomposition reaction can be modified to optimize nanoparticle size, morphology, and composition including the type of inert gas<sup>47,48,50</sup>, peak reaction temperature<sup>44,47–49</sup>, total reaction time<sup>44–46</sup>, and types/ratios of initial chemical compounds utilized in the reaction<sup>20,45,47,48,50</sup>. Salazar-Alvarez et al.<sup>50</sup> and Seo et al.<sup>48</sup> have shown that argon flow during thermal decomposition of MnACAC forms Mn<sub>3</sub>O<sub>4</sub> at lower peak reaction temperatures ranging from 150 °C to 200 °C. When using nitrogen or air, Nolis et al.<sup>47</sup> achieved similar results for MnACAC decomposition where Mn<sub>3</sub>O<sub>4</sub> nanoparticles were produced at lower temperatures (150°C or 200°C) and MnO nanoparticles were generated only at higher temperatures (250 °C and 300 °C)<sup>47</sup>. Higher peak reaction temperatures and longer times held at the peak reaction temperature, also known as the aging time, have also been associated with an increase in nanoparticle size<sup>44–49</sup>. Furthermore, the heating rate of the reaction can impact nanoparticle size. Schladt et al.<sup>44</sup> found that increasing the heating rate from 1.5 °C/min up to 90°C/min dropped nanoparticle size from 18.9 nm to 6.5 nm, respectively. Finally, different chemicals can be added as reducing agents and stabilizers in manganese thermal decomposition reactions; however, OA<sup>20,47,48,50</sup> and oleic acid<sup>20,45</sup> are most commonly used. The ratio of OA to oleic acid has been proven to affect the chemistry and shape of synthesized MnO nanoparticles. According to Zhang et al.<sup>20</sup>, OA only resulted in the formation of Mn<sub>3</sub>O<sub>4</sub> nanoparticles, a combination of OA and oleic acid led to a mixture of Mn<sub>3</sub>O<sub>4</sub> and MnO nanoparticles, and oleic acid only produced MnO nanoparticles. Interestingly, experience shows that MnO nanoparticles can be fabricated with OA only, and that oleic acid is not necessary to

promote formation of the MnO crystalline phase. Furthermore, the use of OA by itself fabricated spherical nanoparticles, while oleic acid alone generated star shaped nanoparticles<sup>20,64</sup>. Clearly, there is much flexibility in altering synthesis parameters to impact resulting physical and chemical properties of MnO nanoparticles.

Despite the detailed protocol, instances may arise that require troubleshooting. The following paragraph details some common issues and solutions. During the reaction, if the temperature seems to stabilize around 100 °C, some water may have leaked into the heating mantle. Visibly inspect the surrounding area for water leakage from the condenser. Do not directly touch the mantle or round bottom flask without heat resistant gloves, as they will be very hot. If water is observed, immediately turn off the temperature controller, unplug the heating mantle, and let it dry overnight. To prevent future leakages, use an interlocked worm gear hose clamp to secure the water tubing to the condenser. In the case that the desired product is MnO, but only Mn<sub>3</sub>O<sub>4</sub> is produced, it is important to check the nitrogen flow during the reaction. The middle bubbler should have a constant stream of bubbles (see the video for correct bubbling rate), while the right bubbler should only have one or two bubbles forming in it. Incorrect nitrogen flow can occur if the differential silicone oil levels in each mineral oil bubbler are not maintained. Check the oil levels before every experiment and fill up the bubblers according to step 1.5 if needed. During nanoparticle collection, the protocol specifies to pour out the supernatant without disturbing the nanoparticle pellet. The best way to discard the supernatant is to pour it out with one fast continuous motion rather than a slow one. However, if the pellet gets easily detached from the centrifuge tube, the use of a transfer pipette is recommended to remove the supernatant. During nanoparticle collection and TEM grid preparation, bath sonication is a key step. If the nanoparticles are not resuspending correctly, move the tube around the water bath sonicator until an area is located where the sonication can be felt by the hand holding the tube. The nanoparticle pellet can also be visibly seen disintegrating under strong bath sonication if the tube is in the correct spot. After nanoparticle resuspension, it is important that the TEM grid is suspended in the air with reverse tweezers rather than placed onto a wipe or directly onto an absorbent bench surface. The wipe or absorbent bench surface will wick the nanoparticle suspension off of the TEM grid before drying, resulting in insufficient nanoparticle deposition on the grid for imaging.

Although the thermal decomposition reaction is fairly simple and straightforward to follow to synthesize MnO nanoparticles, there are some limitations associated with the method. While it is possible to control the physical and chemical properties of nanoparticles to some extent, some variables such as temperature and aging time impact both nanoparticle size and phase composition simultaneously. Therefore, it is difficult to always have precise independent control of nanoparticle properties using this method. In addition, scaling up of the nanoparticle synthesis by tripling or quadrupling the amounts of starting materials can cause the reaction to become unstable and violent. Larger batch size is also associated with a decreased yield. Furthermore, despite storage of MnO nanoparticles inside capped scintillation vials wrapped in paraffin plastic film, we have seen oxidation of the nanoparticle surface to Mn<sub>3</sub>O<sub>4</sub> as evaluated by X-ray photoelectron spectroscopy. Finally, the MnO nanoparticles generated by this technique will be hydrophobic and capped with OA (**Figure 7**). Further surface modification to

transition nanoparticles to a hydrophilic state will need to be applied to enable nanoparticle suspension in aqueous media. Several methods have been established to promote the dispersion of nanoparticles in biological solutions including nanoparticle encapsulation inside of polymers<sup>14</sup>, coating of the nanoparticle surface with lipids<sup>52</sup>, or ligand exchange to substitute the OA on the nanoparticle surface with hydrophilic ligands such as poly(acrylic acid)<sup>20</sup>. To achieve encapsulation of MnO nanoparticles within poly(lactic-co-glycolic acid) (PLGA) polymer, follow McCall and Sirianni's detailed *JoVE* protocol<sup>65</sup>; MnO nanoparticles can be added directly to the PLGA polymer solution as described for hydrophobic drugs in step 8 of the Nanoparticle Preparation section. MnO nanocrystal distribution inside of PLGA nanoparticles can be assessed using TEM and loading of Mn inside the PLGA polymer can be determined by thermogravimetric analysis as shown in Bennewitz et al.<sup>14</sup>.

Although MnO nanoparticles can be utilized for a wide variety of applications due to their magnetic, electronic and catalytic properties, we are interested in applying MnO nanoparticles as switchable, T<sub>1</sub> MRI contrast agents. Previously, our group and others have shown that intact MnO nanoparticles have negligible T<sub>1</sub> MRI contrast (MRI signal is "OFF") at physiological pH 7.4 mimicking the blood<sup>14–19</sup>. However, MnO dissolves to create substantial Mn<sup>2+</sup> ions at low pH 5 mimicking cellular endosomes; released Mn<sup>2+</sup> will coordinate with surrounding water molecules to turn "ON" MRI signal at low pH<sup>14–19</sup>. MnO nanoparticles can be localized to different cells of interest, such as cancer cells, through addition of targeting peptides or antibodies to the nanoparticle surface<sup>51,66</sup>. Here, we describe the synthesis of MnO nanoparticles with an average diameter ranging from 18.6 nm to 38.8 nm. Control of nanoparticle size can be useful for improving MRI contrast agent effectiveness. Specifically, it is anticipated that larger nanoparticles will have more surface area for attachment of targeting ligands to enhance nanoparticle accumulation at the site of interest such as tumors. However, overall nanoparticle size with added surface groups should be limited to 50-100 nm to maximize tumor accumulation<sup>67,68</sup>. Smaller nanoparticles, on the other hand, have a higher surface area-to-volume ratio to facilitate faster release of Mn<sup>2+</sup> under acidic environments and should allow for enhanced nanoparticle packing volumes inside of polymeric delivery systems. Synthesis of MnO over Mn<sub>3</sub>O<sub>4</sub> should also improve MRI contrast, as MnO has been shown to dissolve faster than Mn<sub>3</sub>O<sub>4</sub> in concentrated acidic solutions to generate more Mn<sup>2+</sup> ions<sup>69</sup>. In summary, we have described a thermal decomposition protocol for fabrication of MnO nanoparticles that is relatively straightforward and customizable to allow for optimizing nanoparticle design for future use in applications such as smart MRI contrast agents, biosensors, catalysts, batteries and water purification.

#### ACKNOWLEDGMENTS:

This work was supported by WVU Chemical and Biomedical Engineering Department startup funds (M.F.B.). The authors would like to thank Dr. Marcela Redigolo for guidance on grid preparation and image capture of nanoparticles with TEM, Dr. Qiang Wang for support on evaluating XRD and FTIR spectra, Dr. John Zondlo and Hunter Snoderly for programming and integrating the temperature controller into the nanoparticle synthesis protocol, James Hall for his assistance in assembly of the nanoparticle synthesis setup, Alexander Pueschel and Jenna Vito for aiding in quantification of MnO nanoparticle diameters from TEM images, and the WVU

Shared Research Facility for use of the TEM, XRD, and FTIR.

#### DISCLOSURES:

The authors have nothing to disclose.

#### REFERENCES:

1. Felton, C. et al. Magnetic nanoparticles as contrast agents in biomedical imaging: recent advances in iron- and manganese-based magnetic nanoparticles. *Drug Metabolism Reviews*. **46** (2), 142–154 (2014).
2. Hsu, B.Y.W. et al. Relaxivity and toxicological properties of manganese oxide nanoparticles for MRI applications. *RSC Advances*. **6** (51), 45462–45474 (2019).
3. Wierzbinski, K.R. et al. Potential use of superparamagnetic iron oxide nanoparticles for in vitro and in vivo bioimaging of human myoblasts. *Scientific Reports*. **8** (1), 1–17 (2018).
4. Vukojević, V. et al. Enzymatic glucose biosensor based on manganese dioxide nanoparticles decorated on graphene nanoribbons. *Journal of Electroanalytical Chemistry*. **823**, 610–616 (2018).
5. George, J.M., Antony, A., Mathew, B. Metal oxide nanoparticles in electrochemical sensing and biosensing: a review. *Microchimica Acta*. **185** (7), 358 (2018).
6. Fei, J. et al. Tuning the Synthesis of Manganese Oxides Nanoparticles for Efficient Oxidation of Benzyl Alcohol. *Nanoscale Research Letters*. **12** (2017).
7. Le, T.-H., Ngo, T.H.A., Doan, V.T., Nguyen, L.M.T., Le, M.C. Preparation of Manganese Dioxide Nanoparticles on Laterite for Methylene Blue Degradation. *Journal of Chemistry*. **2019**, e1602752 (2019).
8. Kuo, C.-H. et al. Robust Mesoporous Manganese Oxide Catalysts for Water Oxidation. *ACS Catalysis*. **5** (3), 1693–1699 (2015).
9. Farzana, R., Rajarao, R., Hassan, K., Behera, P.R., Sahajwalla, V. Thermal nanosizing: Novel route to synthesize manganese oxide and zinc oxide nanoparticles simultaneously from spent Zn–C battery. *Journal of Cleaner Production*. **196**, 478–488 (2018).
10. Elbasuney, S., Elsayed, M.A., Mostafa, S.F., Khalil, W.F. MnO<sub>2</sub> Nanoparticles Supported on Porous Al<sub>2</sub>O<sub>3</sub> Substrate for Wastewater Treatment: Synergy of Adsorption, Oxidation, and Photocatalysis. *Journal of Inorganic and Organometallic Polymers and Materials*. (2019).
11. Shapiro, E.M. et al. MRI detection of single particles for cellular imaging. *Proceedings of the National Academy of Sciences*. **101** (30), 10901–10906 (2004).
12. Shapiro, E.M., Skrtic, S., Koretsky, A.P. Sizing it up: Cellular MRI using micron-sized iron oxide particles. *Magnetic Resonance in Medicine*. **53** (2), 329–338 (2005).
13. Bennewitz, M.F., Tang, K.S., Markakis, E.A., Shapiro, E.M. Specific chemotaxis of magnetically labeled mesenchymal stem cells: implications for MRI of glioma. *Molecular imaging and biology: MIB: the official publication of the Academy of Molecular Imaging*. **14** (6), 676–687 (2012).
14. Bennewitz, M.F. et al. Biocompatible and pH-Sensitive PLGA Encapsulated MnO Nanocrystals for Molecular and Cellular MRI. *ACS Nano*. **5** (5), 3438–3446 (2011).
15. Chen, Y. et al. Manganese oxide-based multifunctionalized mesoporous silica nanoparticles for pH-responsive MRI, ultrasonography and circumvention of MDR in cancer cells. *Biomaterials*. **33** (29), 7126–7137 (2012).

16. Park, M. et al. Large-Scale Synthesis of Ultrathin Manganese Oxide Nanoplates and Their Applications to T1 MRI Contrast Agents. *Chemistry of Materials*. **23** (14), 3318–3324 (2011).
17. Duan, B. et al. Core–Shell Structurized Fe<sub>3</sub>O<sub>4</sub>@C@MnO<sub>2</sub> Nanoparticles as pH Responsive T1-T2\* Dual-Modal Contrast Agents for Tumor Diagnosis. *ACS Biomaterials Science & Engineering*. **4** (8), 3047–3054 (2018).
18. Hao, Y. et al. Multifunctional nanosheets based on folic acid modified manganese oxide for tumor-targeting theranostic application. *Nanotechnology*. **27** (2), 025101 (2015).
19. Shi, Y., Guenneau, F., Wang, X., H  lary, C., Coradin, T. MnO<sub>2</sub>-gated Nanoplatfoms with Targeted Controlled Drug Release and Contrast-Enhanced MRI Properties: from 2D Cell Culture to 3D Biomimetic Hydrogels. *Nanotheranostics*. **2** (4), 403–416 (2018).
20. Zhang, H. et al. Revisiting the coordination chemistry for preparing manganese oxide nanocrystals in the presence of oleylamine and oleic acid. *Nanoscale*. **6** (11), 5918 (2014).
21. McDonagh, B.H. et al. L-DOPA-Coated Manganese Oxide Nanoparticles as Dual MRI Contrast Agents and Drug-Delivery Vehicles. *Small*. **12** (3), 301–306 (2016).
22. Ding, X. et al. Polydopamine coated manganese oxide nanoparticles with ultrahigh relaxivity as nanotheranostic agents for magnetic resonance imaging guided synergetic chemo-/photothermal therapy. *Chemical Science*. **7** (11), 6695–6700 (2016).
23. Wei, R. et al. Versatile Octapod-Shaped Hollow Porous Manganese(II) Oxide Nanoplatfom for Real-Time Visualization of Cargo Delivery. *Nano Letters*. **19** (8), 5394–5402 (2019).
24. Na, H.B. et al. Development of a T1 contrast agent for magnetic resonance imaging using MnO nanoparticles. *Angewandte Chemie (International Ed. in English)*. **46** (28), 5397–5401 (2007).
25. Rockenberger, J., Scher, E.C., Alivisatos, A.P. A New Nonhydrolytic Single-Precursor Approach to Surfactant-Capped Nanocrystals of Transition Metal Oxides. *Journal of the American Chemical Society*. **121** (49), 11595–11596 (1999).
26. Han, C. et al. Synthesis of a multifunctional manganese(II)–carbon dots hybrid and its application as an efficient magnetic-fluorescent imaging probe for ovarian cancer cell imaging. *Journal of Materials Chemistry B*. **4** (35), 5798–5802 (2016).
27. Wang, A. et al. Redox-mediated dissolution of paramagnetic nanolids to achieve a smart theranostic system. *Nanoscale*. **6** (10), 5270–5278 (2014).
28. Jia, Q. et al. A Magnetofluorescent Carbon Dot Assembly as an Acidic H<sub>2</sub>O<sub>2</sub>-Driven Oxygenerator to Regulate Tumor Hypoxia for Simultaneous Bimodal Imaging and Enhanced Photodynamic Therapy. *Advanced Materials*. **30** (13), 1706090 (2018).
29. Yang, B. et al. A three dimensional Pt nanodendrite/graphene/MnO<sub>2</sub> nanoflower modified electrode for the sensitive and selective detection of dopamine. *Journal of Materials Chemistry B*. **3** (37), 7440–7448 (2015).
30. Li, J., Li, D., Yuan, R., Xiang, Y. Biodegradable MnO<sub>2</sub> Nanosheet-Mediated Signal Amplification in Living Cells Enables Sensitive Detection of Down-Regulated Intracellular MicroRNA. *ACS Applied Materials & Interfaces*. **9** (7), 5717–5724 (2017).
31. Fan, H. et al. A Smart DNAzyme–MnO<sub>2</sub> Nanosystem for Efficient Gene Silencing. *Angewandte Chemie International Edition*. **54** (16), 4801–4805 (2015).
32. Zhang, Y. et al. A real-time fluorescence turn-on assay for acetylcholinesterase activity based on the controlled release of a perylene probe from MnO<sub>2</sub> nanosheets. *Journal of Materials Chemistry C*. **5** (19), 4691–4694 (2017).

33. Meng, H.-M. et al. Multiple Functional Nanoprobe for Contrast-Enhanced Bimodal Cellular Imaging and Targeted Therapy. *Analytical Chemistry*. **87** (8), 4448–4454 (2015).
34. Zhao, Z. et al. Activatable Fluorescence/MRI Bimodal Platform for Tumor Cell Imaging via MnO<sub>2</sub> Nanosheet–Aptamer Nanoprobe. *Journal of the American Chemical Society*. **136** (32), 11220–11223 (2014).
35. Chen, J.-L. et al. A glucose-activatable trimodal glucometer self-assembled from glucose oxidase and MnO<sub>2</sub> nanosheets for diabetes monitoring. *Journal of Materials Chemistry B*. **5** (27), 5336–5344 (2017).
36. Yang, G. et al. Hollow MnO<sub>2</sub> as a tumor-microenvironment-responsive biodegradable nano-platform for combination therapy favoring antitumor immune responses. *Nature Communications*. **8** (1), 1–13 (2017).
37. Wu, Y. et al. Versatile in situ synthesis of MnO<sub>2</sub> nanolayers on upconversion nanoparticles and their application in activatable fluorescence and MRI imaging. *Chemical Science*. **9** (24), 5427–5434 (2018).
38. Jing, X. et al. Intelligent nanoflowers: a full tumor microenvironment-responsive multimodal cancer theranostic nanoplatform. *Nanoscale*. **11** (33), 15508–15518 (2019).
39. Peng, Y.-K. et al. Engineered core–shell magnetic nanoparticle for MR dual-modal tracking and safe magnetic manipulation of ependymal cells in live rodents. *Nanotechnology*. **29** (1), 015102 (2018).
40. Ren, S. et al. Ternary-Responsive Drug Delivery with Activatable Dual Mode Contrast-Enhanced in vivo Imaging. *ACS Applied Materials & Interfaces*. **10** (38), 31947–31958 (2018).
41. Zhen, W. et al. Multienzyme-Mimicking Nanocomposite for Tumor Phototheranostics and Normal Cell Protection. *ChemNanoMat*. **5** (1), 101–109 (2019).
42. Tang, W. et al. Wet/Sono-Chemical Synthesis of Enzymatic Two-Dimensional MnO<sub>2</sub> Nanosheets for Synergistic Catalysis-Enhanced Phototheranostics. *Advanced Materials*. **31** (19), 1900401 (2019).
43. Ding, B., Zheng, P., Ma, P., Lin, J. Manganese Oxide Nanomaterials: Synthesis, Properties, and Theranostic Applications. *Advanced Materials*. 1905823 (2020).
44. Schladt, T.D., Graf, T., Tremel, W. Synthesis and Characterization of Monodisperse Manganese Oxide Nanoparticles–Evaluation of the Nucleation and Growth Mechanism. *Chemistry of Materials*. **21** (14), 3183–3190 (2009).
45. Yin, M., O’Brien, S. Synthesis of Monodisperse Nanocrystals of Manganese Oxides. *Journal of the American Chemical Society*. **125** (34), 10180–10181 (2003).
46. Chen, Y., Johnson, E., Peng, X. Formation of Monodisperse and Shape-Controlled MnO Nanocrystals in Non-Injection Synthesis: Self-Focusing via Ripening. *Journal of the American Chemical Society*. **129** (35), 10937–10947 (2007).
47. Nolis, G.M., Bolotnikov, J.M., Cabana, J. Control of Size and Composition of Colloidal Nanocrystals of Manganese Oxide. *Inorganic Chemistry*. **57** (20), 12900–12907 (2018).
48. Seo, W.S. et al. Size-Dependent Magnetic Properties of Colloidal Mn<sub>3</sub>O<sub>4</sub> and MnO Nanoparticles. *Angewandte Chemie International Edition*. **43** (9), 1115–1117 (2004).
49. Douglas, F.J. et al. Formation of octapod MnO nanoparticles with enhanced magnetic properties through kinetically-controlled thermal decomposition of polynuclear manganese complexes. *Nanoscale*. **6** (1), 172–176 (2013).
50. Salazar-Alvarez, G., Sort, J., Suriñach, S., Baró, M.D., Nogués, J. Synthesis and Size-

- Dependent Exchange Bias in Inverted Core-Shell MnO|Mn<sub>3</sub>O<sub>4</sub> Nanoparticles. *Journal of the American Chemical Society*. **129** (29), 9102–9108 (2007).
51. Zhang, T., Ge, J., Hu, Y., Yin, Y. A General Approach for Transferring Hydrophobic Nanocrystals into Water. *Nano Letters*. **7** (10), 3203–3207 (2007).
52. Chhour, P. et al. Nanodisco balls: control over surface versus core loading of diagnostically active nanocrystals into polymer nanoparticles. *ACS nano*. **8** (9), 9143–9153 (2014).
53. Suk, J.S., Xu, Q., Kim, N., Hanes, J., Ensign, L.M. PEGylation as a strategy for improving nanoparticle-based drug and gene delivery. *Advanced Drug Delivery Reviews*. **99**, 28–51 (2016).
54. Huang, C.-C., Khu, N.-H., Yeh, C.-S. The characteristics of sub 10 nm manganese oxide T1 contrast agents of different nanostructured morphologies. *Biomaterials*. **31** (14), 4073–4078 (2010).
55. Zhao, N. et al. Shape- and Size-Controlled Synthesis and Dependent Magnetic Properties of Nearly Monodisperse Mn<sub>3</sub>O<sub>4</sub> Nanocrystals. *Small*. **4** (1), 77–81 (2008).
56. He, D., Hai, L., He, X., Yang, X., Li, H.-W. Glutathione-Activatable and O<sub>2</sub>/Mn<sup>2+</sup>-Evolving Nanocomposite for Highly Efficient and Selective Photodynamic and Gene-Silencing Dual Therapy. *Advanced Functional Materials*. **27** (46), 1704089 (2017).
57. He, D. et al. Redox-responsive degradable honeycomb manganese oxide nanostructures as effective nanocarriers for intracellular glutathione-triggered drug release. *Chemical Communications*. **51** (4), 776–779 (2015).
58. Chen, Y. et al. Multifunctional Graphene Oxide-based Triple Stimuli-Responsive Nanotheranostics. *Advanced Functional Materials*. **24** (28), 4386–4396 (2014).
59. Prasad, P. et al. Multifunctional Albumin–MnO<sub>2</sub> Nanoparticles Modulate Solid Tumor Microenvironment by Attenuating Hypoxia, Acidosis, Vascular Endothelial Growth Factor and Enhance Radiation Response. *ACS Nano*. **8** (4), 3202–3212 (2014).
60. Perez De Berti, I. et al. Alternative low-cost approach to the synthesis of magnetic iron oxide nanoparticles by thermal decomposition of organic precursors. *Nanotechnology*. **24**, 175601 (2013).
61. Mourdikoudis, S., Liz-Marzán, L.M. Oleylamine in Nanoparticle Synthesis. *Chemistry of Materials*. **25** (9), 1465–1476 (2013).
62. Zheng, M. et al. A simple additive-free approach for the synthesis of uniform manganese monoxide nanorods with large specific surface area. *Nanoscale Research Letters*. **8** (1), 166 (2013).
63. Xu, Z., Shen, C., Hou, Y., Gao, H., Sun, S. Oleylamine as Both Reducing Agent and Stabilizer in a Facile Synthesis of Magnetite Nanoparticles. *Chemistry of Materials*. **21** (9), 1778–1780 (2009).
64. Hou, Y., Xu, Z., Sun, S. Controlled Synthesis and Chemical Conversions of FeO Nanoparticles. *Angewandte Chemie*. **119** (33), 6445–6448 (2007).
65. McCall, R.L., Sirianni, R.W. PLGA Nanoparticles Formed by Single- or Double-emulsion with Vitamin E-TPGS. *Journal of Visualized Experiments*. (82) (2013).
66. Le Joncour, V., Laakkonen, P. Seek & Destroy, use of targeting peptides for cancer detection and drug delivery. *Bioorganic & Medicinal Chemistry*. **26** (10), 2797–2806 (2018).
67. Perry, J.L. et al. Mediating Passive Tumor Accumulation through Particle Size, Tumor Type, and Location. *Nano Letters*. **17** (5), 2879–2886 (2017).
68. Tang, L. et al. Investigating the optimal size of anticancer nanomedicine. *Proceedings of the*



1011 *National Academy of Sciences*. **111** (43), 15344–15349 (2014).  
1012 69. Godunov, E.B., Izotov, A.D., Gorichev, I.G. Dissolution of Manganese Oxides of Various  
1013 Compositions in Sulfuric Acid Solutions Studied by Kinetic Methods. *Inorganic Materials*. **54** (1),  
1014 66–71 (2018).  
1015

Figure 1

[Click here to access/download;Figure;Figure 1.pdf](#)

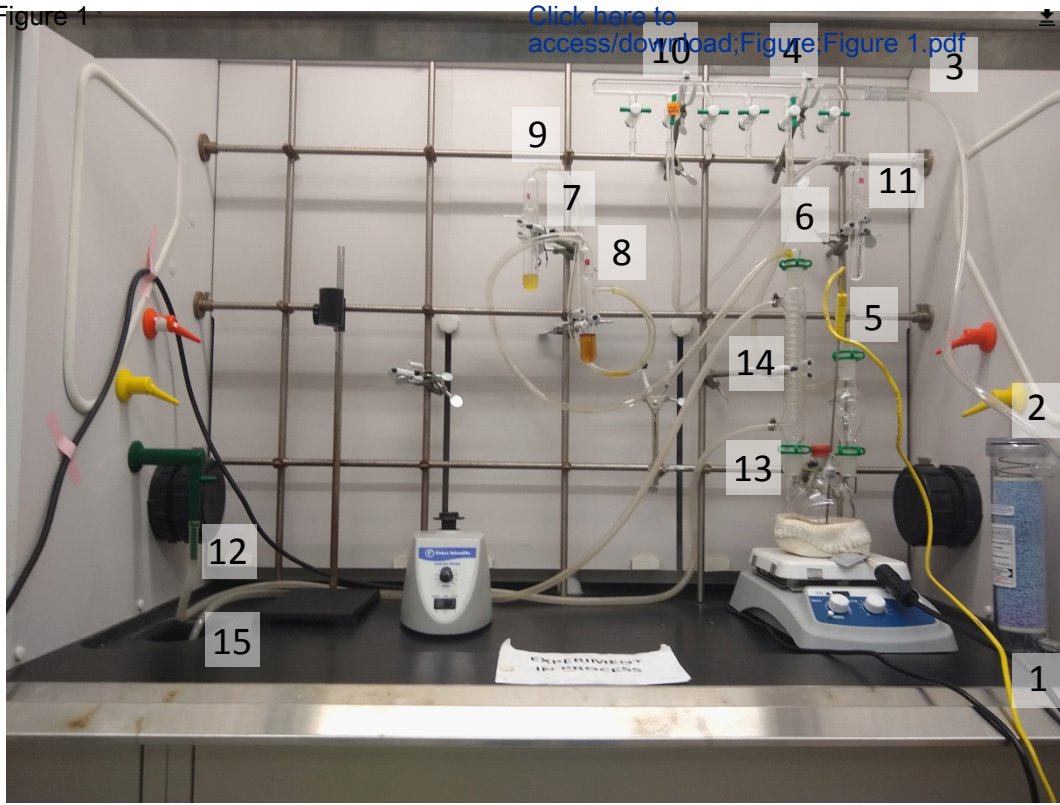
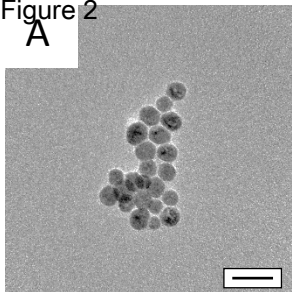


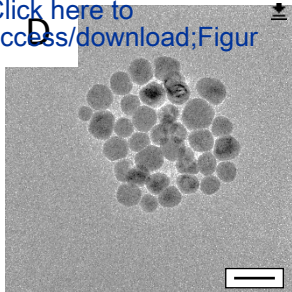
Figure 2

A

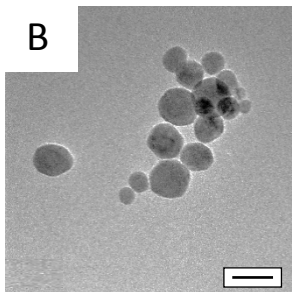


[Click here to access/download;Figur](#)

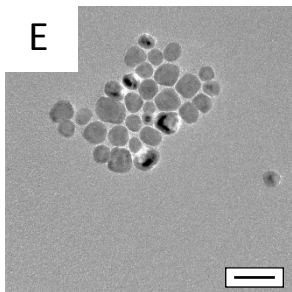
D



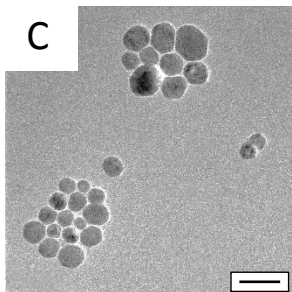
B



E



C



F

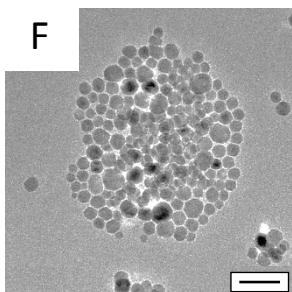
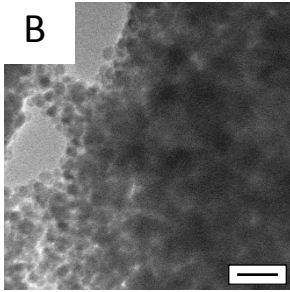
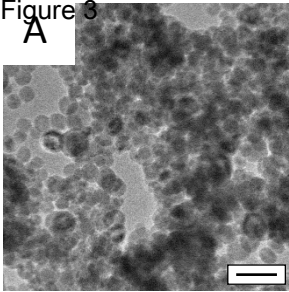


Figure 3



[Click here to access/download:Figure;Figure 3.pdf](#)

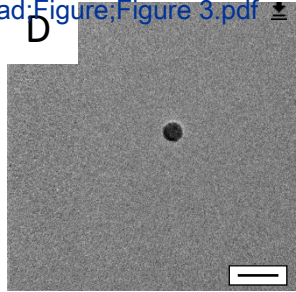
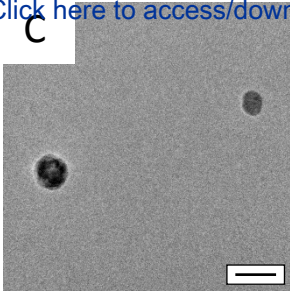
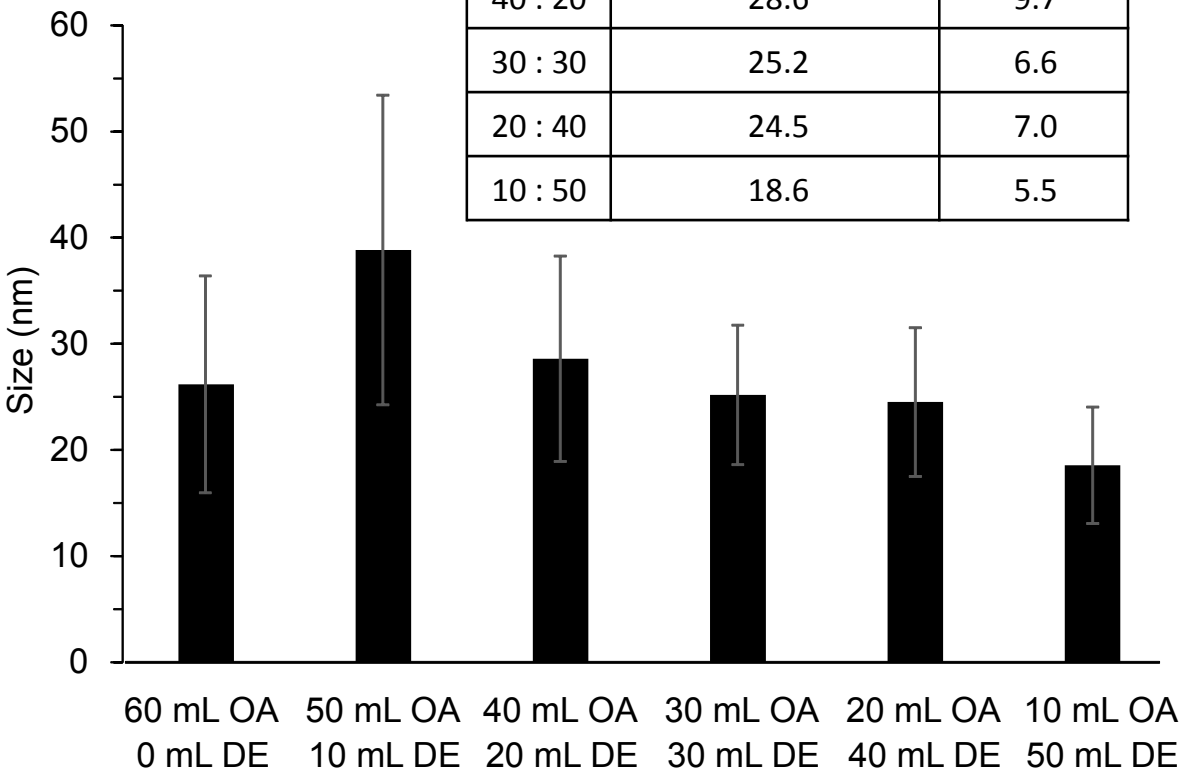


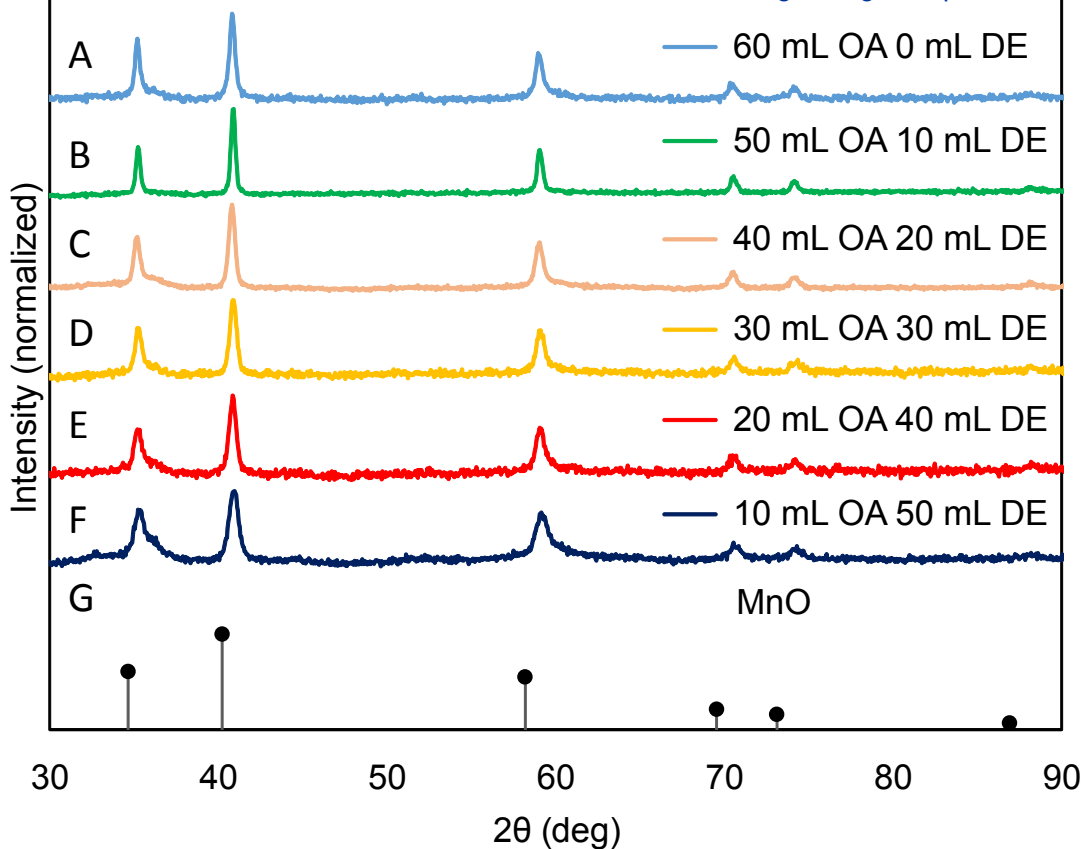
Figure 4



[Click here to access/download;Figure;Figure 4.pdf](#)



Figure 5

[Click here to](#)[access/download;Figure;Figure 5.pdf](#)

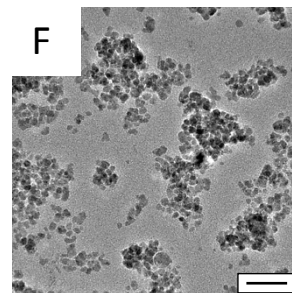
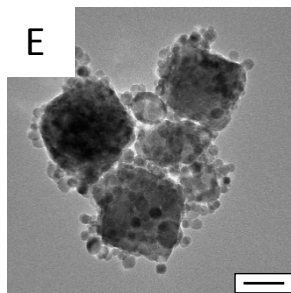
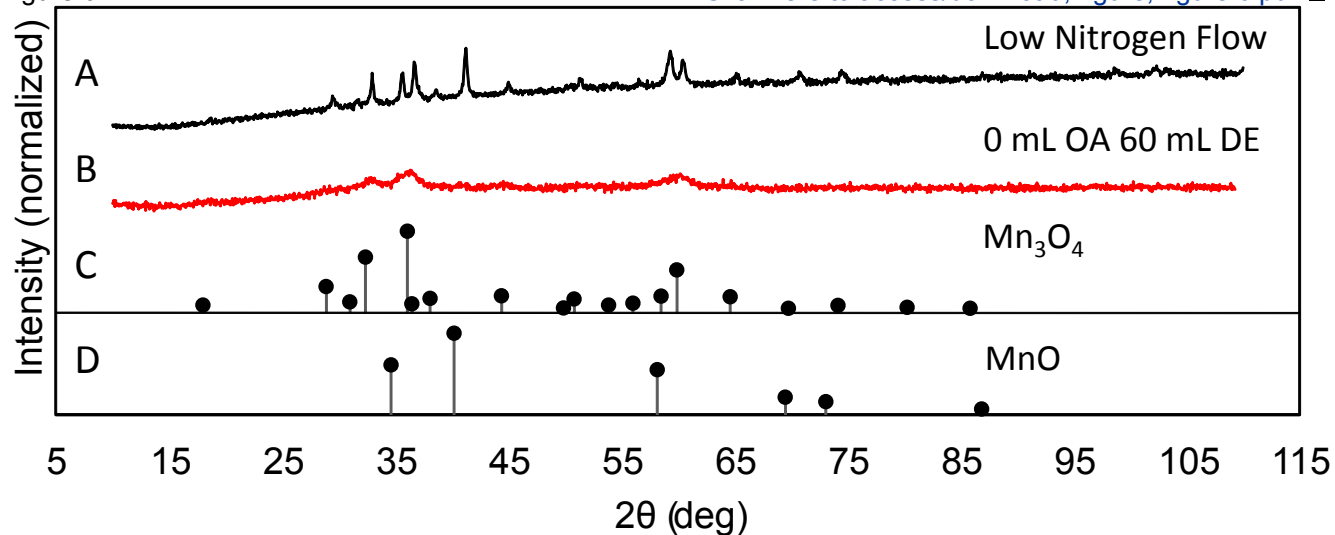
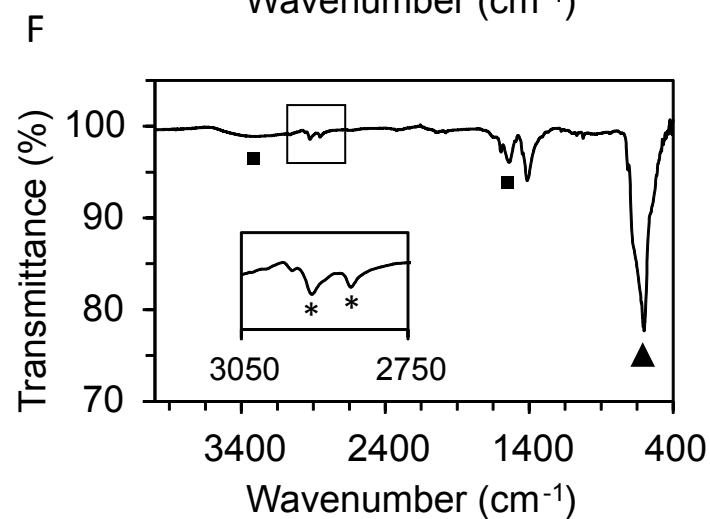
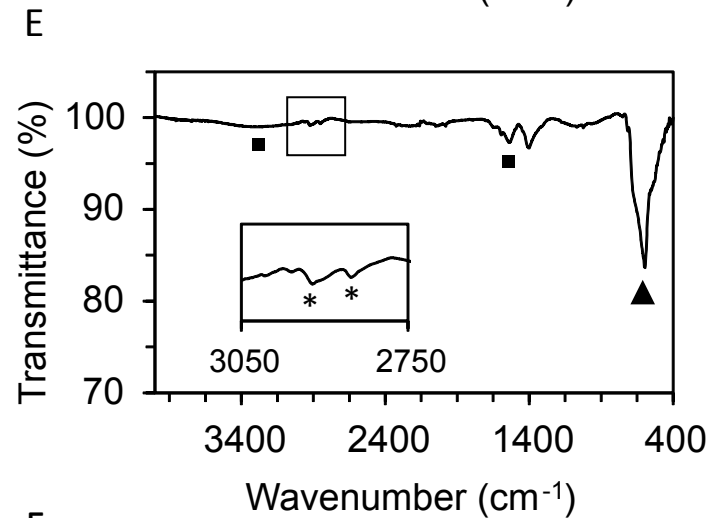
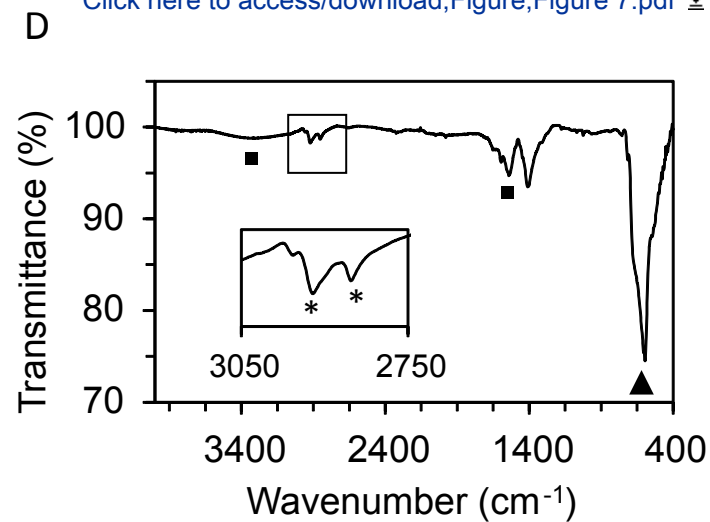
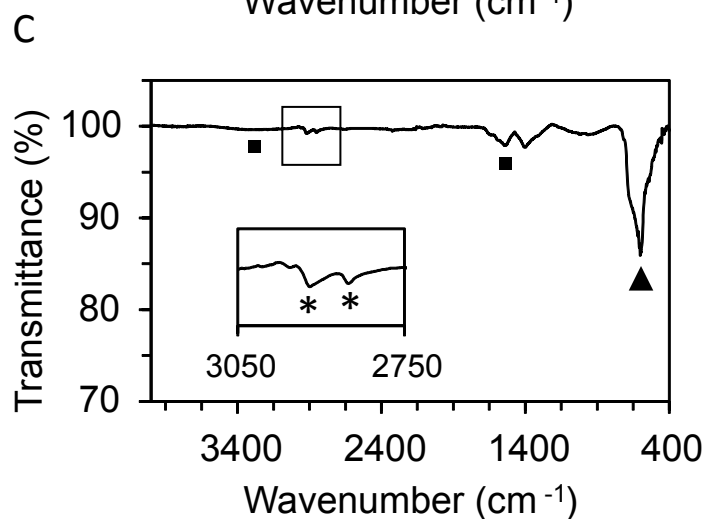
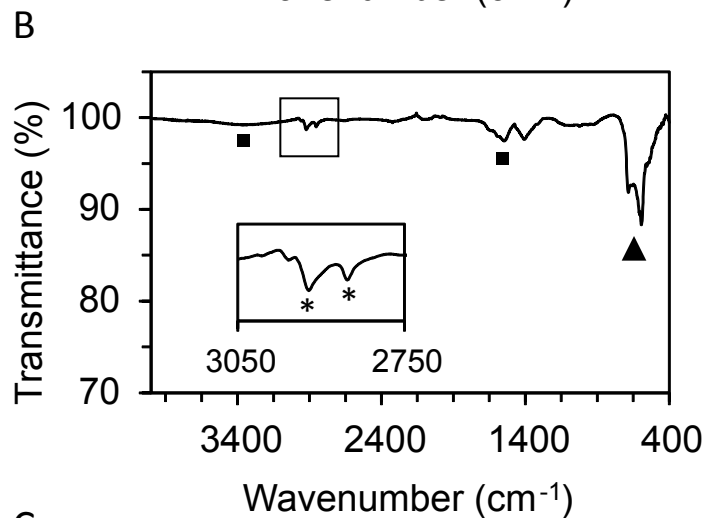
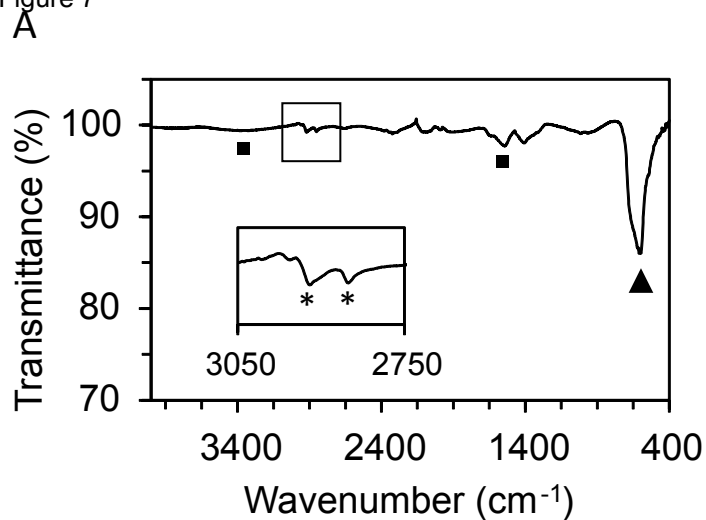


Figure 7

[Click here to access/download;Figure;Figure 7.pdf](#)



Item Name	Company	Catalog Number	Description
<b>Chemicals and Gases</b>			
Benzyl ether (DE)	Acros Organics	AC14840-0010	Concentration: 99%, 1 L
Drierite	W. A. Hammond Drierite Co. LTD	23001	Drierite 8 mesh, 1 lb
Ethanol	Decon Laboratories	2701	200 proof, 4 x 3.7 L
Hexane	Macron Fine Chemicals	5189-08	Concentration: $\geq 98.5\%$ , 4 L
Hydrochloric acid	VWR	BDH3030-2.5LPC	Concentration: 36.5 - 38.0 % ACS, 2.5 L
Manganese (II) acetyl acetonate (Mn(II)ACAC)	Sigma Aldrich	245763-100G	100 g
Nitrogen gas tank	Airgas	NI R300	Research 5.7 grade nitrogen, size 300 cylinder
Nitrogen regulator	Airgas	Y11244D580-AG	Single stage brass 0-100 psi analytical cylinder regulator CGA-580 with needle outlet
Oleylamine (OA)	Sigma Aldrich	O7805-500G	Concentration: 70%, technical grade, 500 g
Silicone oil	Beantown Chemical	221590-100G	100 g
<b>Equipment</b>			
Centrifuge	Beckman-Coulter	Avanti J-E	JA-20 fixed-angle aluminum rotor, 8 x 50 mL, 48,400 x g
Hemisphere mantle	Ace Glass Inc.	12035-17	115 V, 270 W, 500 mL, temperature up to 450 °C
Hot plate stirrer	VWR	97042-642	120 V, 1000 W, 8.3 A, ceramic top
Temperature controller	Yokogawa Electric Corporation	UP351	
Temperature probe	Omega	KMQXL-040G-12	Immersion probe, temperature up to 1335 °C
Vacuum oven	Fisher Scientific	282A	120 V, 1800 W, temperature up to 280 °C
Vortex mixer	Fisher Scientific	02-215-365	120 V, 50/60 Hz, 150 W
Water bath sonicator	Fisher Scientific	FS30H	Ultrasonic power 130 W, 3.7 L tank
<b>Tools and Materials</b>			
Dumont tweezer	Electron Microscopy Sciences	72703D	Style 5/45, Dumoxel, 109 mm, for picking up TEM grids

Dumont reverse tweezer	Ted Pella	5748	Style N2a, 118 mm, NM-SS, self-closing, holding TEM grids in place for sample preparation
Mortar and pestle	Amazon	BS0007	BIPEE agate mortar and pestle, 70 X 60 X 15 mm labware
Nalgene™ Oak Ridge tubes	ThermoFisher Scientific	3139-0050	Polypropylene copolymer, 50,000 x g, 50 mL, pack of 10
Scintillation vials	Fisher Scientific	03-337-4	20 mL vials with white caps, case of 500
TEM grids	Ted Pella	01813-F	Carbon Type-B, 300 mesh, copper, pack of 50
<b>Glassware Setup</b>			
4-neck round bottom flask	Chemglass Life Sciences	CG-1534-01	24/40 joint, 500 mL, #7 chem thread for thermometers
6-port vacuum manifold	Chemglass Life Sciences	CG-4430-02	480 nm, 6 ports, 4 mm PTFE stopcocks
Adapter	Chemglass Life Sciences	CG-1014-01	24/40 inner joint, 90°
Condenser	Chemglass Life Sciences	CG-1216-03	24/40 joint, 365 mm, 250 mm jacket length
Drierite 26800 drying column	Cole-Parmer	EW-07193-00	200 L/hr, 90 psi
Funnel	Chemglass Life Sciences	CG-1720-L-02	24/40 joint, 100 powder funnel, 195 mm OAL
Interlocked worm gear hose clamp	Grainger	16P292	1/2" wide stainless steel clamp, 3/8" to 7/8" diameter, to secure condenser tubing, 10 pack
Keck clips	Kemtech America Inc	CS002440	24/40 joint
Metal claw clamp	Fisher Scientific	05-769-7Q	22cm, three-prong extension clamps
Metal claw clamp holder	Fisher Scientific	05-754Q	Clamp regular holder
Mineral oil bubbler	Kemtech America Inc	B257040	185 mm
Rotovap trap	Chemglass Life Sciences	CG-1319-02	24/40 joints, 100 mL, self washing rotary evaporator
Rubber stopper	Chemglass Life Sciences	CG-3022-98	24/40 joints, red rubber
Tubing for air/water	McMaster-Carr	6516T21	Clear Tygon PVC for air/water, B-44-3, 1/4" ID, 1/16" wall, 25 ft
Tubing for air/water	McMaster-Carr	6516T26	Clear Tygon PVC for air/water, B-44-3, 3/8" ID, 1/16" wall, 25 ft
Tubing for chemicals	McMaster-Carr	5155T34	Clear Tygon PVC for chemicals, E-3603, 3/8" ID, 1/16" wall, 50 ft

<b>Analysis Programs</b>			
XRD analysis program	Malvern Panalytical	N/A	X'Pert HighScore Plus
FTIR analysis program	Varian, Inc.	N/A	Varian Resolutions Pro

## Response to Editor's Comments

\*All changes to the revised text are shown in the track changes function.

1. Please take this opportunity to thoroughly proofread the manuscript to ensure that there are no spelling or grammar issues. The JoVE editor will not copy-edit your manuscript and any errors in the submitted revision may be present in the published version.

*We have thoroughly read through the entire manuscript again to ensure that there are no spelling or grammar issues.*

2. Please format the manuscript as: paragraph Indentation: 0 for both left and right and special: none, Line spacings: single. Please include a single line space between each step, substep and note in the protocol section. Please use Calibri 12 points

*The manuscript has been reformatted to reflect the desired JoVE specifications outlined above for item 2.*

3. Please ensure that the summary is no more than 50 word limit.

*The summary is 45 words.*

4. JoVE cannot publish manuscripts containing commercial language. Please remove all commercial language from your manuscript and use generic terms instead. All commercial products should be sufficiently referenced in the Table of Materials and Reagents.

For example: Model UP351 from Yokogawa Electric Corporation, Oak Ridge centrifuge tubes, Varian Resolution Pro program, etc.

*All commercialized language has been removed from our manuscript including the temperature controller, drierite, Keck clips, parafilm, Oak Ridge centrifuge tubes, Microsoft Excel, X'Pert High Score Plus program, Varian Resolution Pro program, and Falcon tubes. The X'Pert High Score Plus program and Varian Resolution Pro program have been added to the Table of Materials.*

5. Please ensure that all text in the protocol section is written in the imperative tense as if telling someone how to do the technique (e.g., "Do this," "Ensure that," etc.). The actions should be described in the imperative tense in complete sentences wherever possible. Avoid usage of phrases such as "could be," "should be," and "would be" throughout the Protocol. Any text that cannot be written in the imperative tense may be added as a "Note."

*Passive steps within the protocol have been reworded to be in the imperative tense to tell the reader to do something or have been moved to the "NOTE" category.*

6. The Protocol should contain only action items that direct the reader to do something.

*Passive steps within the protocol have been reworded to be in the imperative tense to tell the reader to do something or have been moved to the "NOTE" category.*

7. Please ensure that individual steps of the protocol should only contain 2-3 actions sentences per step.

*Steps were separated to ensure that there were no more than 2-3 action sentences per step.*

8. Please ensure you answer the "how" question, i.e., how is the step performed?

*Further detail has been added to the temperature increasing steps of nanoparticle synthesis as detailed in our response to point 9. Through changing the passive text to imperative instructions, the actions for the originally passive steps have been better emphasized as to what the reader is to do. Reviewers commented that the protocol was well-written and well explained in the original version. Please let us know if any steps remain that are unclear. We are happy to provide further edits if needed.*

9. 3: where will you observe this temperature increase? What will happen to the substrate during this time? What do you see/observe visually?

*Additional details have been added to the nanoparticle synthesis steps 3.1 to 3.5 to include how the color of the reaction changes from dark brown to green and also that the temperature changes will be observable on the temperature controller display. We have also specified that in stage 3, the mixture will begin to evaporate and that readers should ensure the water is flowing through the condenser sufficiently.*

10. There is a 10-page limit for the Protocol, but there is a 2.75-page limit for filmable content. Please highlight 2.75 pages or less of the Protocol (including headings and spacing) that identifies the essential steps of the protocol for the video, i.e., the steps that should be visualized to tell the most cohesive story of the Protocol.

*Some highlighted text was removed to ensure that there is approximately 2.75 pages highlighted (highlighted portions of the steps were pasted into a separate word document to check for length).*

11. Please obtain explicit copyright permission to reuse any figures from a previous publication. Explicit permission can be expressed in the form of a letter from the editor or a link to the editorial policy that allows re-prints. Please upload this information as a .doc or .docx file to your Editorial Manager account. The Figure must be cited appropriately in the Figure Legend, i.e. "This figure has been modified from [citation]."

*All figures in our manuscript are original and have not been part of a previous publication. No copyright permission is necessary.*

12. As we are a methods journal, please ensure the Discussion explicitly cover the following in detail in 3-6 paragraphs with citations:

- a) Critical steps within the protocol
- b) Any modifications and troubleshooting of the technique
- c) Any limitations of the technique
- d) The significance with respect to existing methods
- e) Any future applications of the technique

*The Discussion meets the criteria of JoVE; there are a total of 6 paragraphs. Paragraphs 1 and 2 discuss critical steps within the protocol and several variables to control to ensure production of uniform nanoparticles with the MnO crystalline phase. Paragraph 3 details different strategies to modify the protocol. Paragraph 4 was added to the Discussion to note various techniques for protocol troubleshooting. Paragraph 5 outlines the limitations of the thermal decomposition method and paragraph 6 describes applications of MnO nanoparticles as contrast agents for magnetic resonance imaging (MRI). The significance of thermal decomposition with respect to existing methods was thoroughly discussed in the Introduction section and was thus not repeated in the Discussion.*

*Paragraph 4 on troubleshooting was added to the revised manuscript and states: "Despite the detailed protocol, instances may arise that require troubleshooting. The following paragraph details some common issues and solutions. During the reaction, if the temperature seems to stabilize around 100°C, some water may have leaked into the heating mantle. Visibly inspect the surrounding area for water leakage from the condenser. Do not directly touch the mantle or round bottom flask without heat resistant gloves, as they will be very hot. If water is observed, immediately turn off the temperature controller, unplug the heating mantle, and let it dry overnight. To prevent future leakages, use an interlocked worm gear hose clamp to secure the water tubing to the condenser. In the case that the desired product is MnO, but only Mn<sub>3</sub>O<sub>4</sub> is produced, it is important to check the nitrogen flow during the reaction. The middle bubbler should have a constant stream of bubbles (see JoVE video for correct bubbling rate), while the right bubbler should only have one or two bubbles forming in it. Incorrect nitrogen flow can occur if the differential silicone oil levels in each mineral oil bubbler are not maintained. Check the oil levels before every experiment and fill up the bubblers according to step 1.5 if needed. During nanoparticle collection, the protocol specifies to pour out the supernatant without disturbing the nanoparticle pellet. The best way to discard the supernatant is to pour it out with one fast continuous motion rather than a slow one. However, if the pellet gets easily detached from the centrifuge tube, the use of a transfer pipette is recommended to remove the supernatant. During nanoparticle collection and TEM grid preparation, bath sonication is a key step. If the nanoparticles are not resuspending correctly, move the tube around the water bath sonicator until an area is located where the sonication can be felt by the hand holding the tube. The nanoparticle pellet can also be visibly seen disintegrating under strong bath sonication if the tube is in the correct spot. After nanoparticle resuspension, it is important that the TEM grid is suspended in the air with reverse tweezers rather than placed onto a wipe or directly onto an absorbent bench surface. The wipe or absorbent bench surface will wick the nanoparticle suspension off of the TEM grid before drying, resulting in insufficient nanoparticle deposition on the grid for imaging."*

## **Response to Reviewers' Comments**

\*All changes to the revised text are shown in the track changes function.

**Reviewer #1:** The authors of the present study presented a protocol that describes a one-pot synthesis of MnO nanoparticles formed by thermal decomposition of manganese(II) acetylacetonate in oleylamine and dibenzyl ether. This is a new protocol that can be applied for the future developments due to the efficacy and simplicity. The manuscript is well-written and well-presented. Therefore, the quality of this manuscript guarantees its publication without further revisions.

*Reviewer 1 noted no major or minor concerns.*

**Reviewer #2:** This JOVE article concerns the synthesis and characterization of manganese oxide nanoparticles. Overall, I found the experiments to be extremely well explained and I think that there are a lot of points here which would be useful to many workers. I have a few minor points to be addressed, which I note below.

Major Concerns:

None

Minor Concerns:

1. constant dark contrast - should be noted as negative contrast (or image darkening). Also, not constant, will decay over days/weeks. You might modify to something like 'constant over typical experimental timeframes'. Bright contrast - positive contrast (brightness in images)

*Dark contrast was changed to “negative contrast” and bright contrast was changed to “positive contrast” in all places in the main text. As suggested, we have modified the sentence at the beginning of the Abstract to read “While iron oxide nanoparticles provide constant negative contrast on MRI over typical experimental timeframes, MnO generates switchable positive contrast on MRI through dissolution of MnO to Mn<sup>2+</sup> at low pH within cell endosomes to ‘turn ON’ MRI contrast.” We also modified another sentence at the beginning of the Introduction to reflect the same idea: “Iron oxide nanoparticles produce robust negative contrast on T<sub>2</sub>\* MRI and are powerful enough to visualize single labeled cells in vivo<sup>11–13</sup>; however, the negative MRI signal cannot be modulated and remains “ON” throughout the duration of typical experiments.”*

2. 'Improperly secured gas cylinders can become airborne if tipped over.' - not sure this quite makes sense. Would revise to something like 'Gas cylinders must be properly secured since they can be very dangerous if tipped over.'

*Step 1.1 was reworded to state “CAUTION: Gas cylinders must be properly secured since they can be very dangerous if tipped over.”*

3. There is something of an incongruity that the authors describe the potential use of the NP as for MRI, but the NP made are hydrophobic, thus cannot be dispersed in water and use for MRI. It would be worth adding a least a brief or simple method to disperse in water, e.g. using lipids.

*We have previous experience in encapsulating MnO nanoparticles within poly(lactic-co-glycolic acid) (PLGA) to make hydrophilic nanoparticles. Dr. Bennewitz was trained in the same laboratory as Dr. Rachel Sirianni and has used a similar encapsulation protocol as outlined in Dr. Sirianni’s JoVE manuscript entitled, “PLGA Nanoparticles Formed by Single- or Double-emulsion with Vitamin E-TPGS”. A section has been added at the end of the limitations paragraph in the Discussion to refer readers to Dr. Sirianni’s JoVE protocol for detailed instructions on MnO nanoparticle encapsulation in PLGA: “To achieve encapsulation of MnO nanoparticles within poly(lactic-co-glycolic acid) (PLGA) polymer, follow McCall and Sirianni’s <sup>65</sup>detailed JoVE protocol; MnO nanoparticles can be added directly to the PLGA polymer solution as described for hydrophobic drugs in step 8 of the Nanoparticle Preparation section. MnO nanocrystal distribution inside of PLGA nanoparticles can be assessed using TEM and loading of Mn inside the PLGA polymer can be determined by thermogravimetric analysis as shown in Bennewitz et al.<sup>14</sup>”*

Figure S1

[Click here to  
access/download;Supplemental File](#)

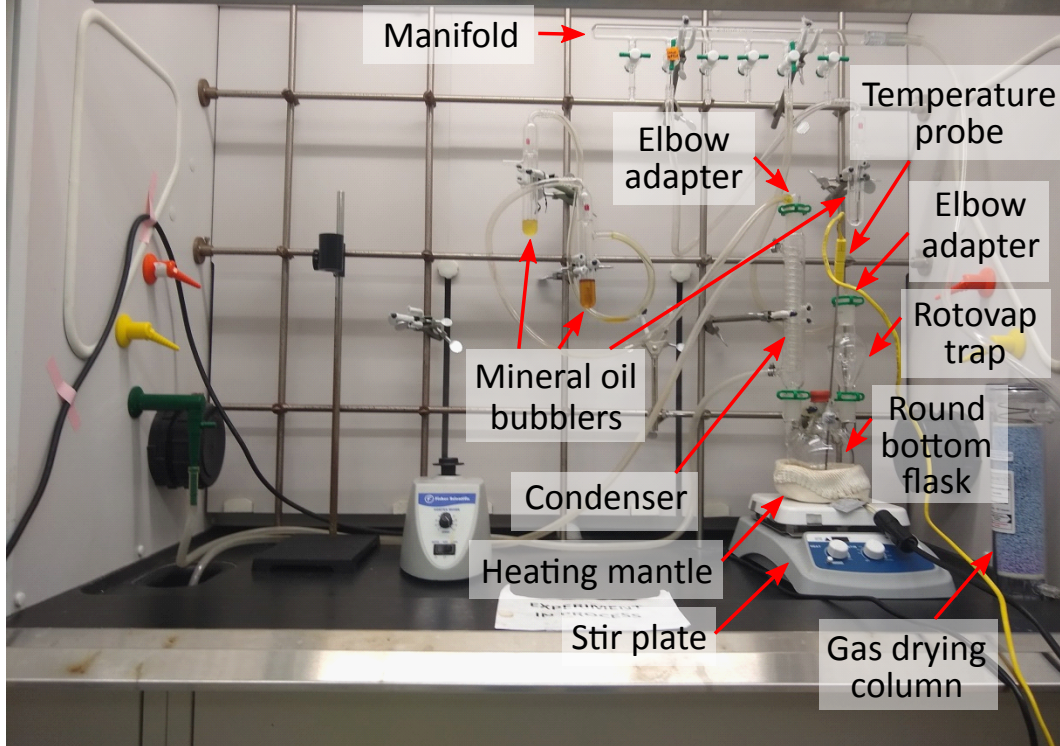


Figure S2

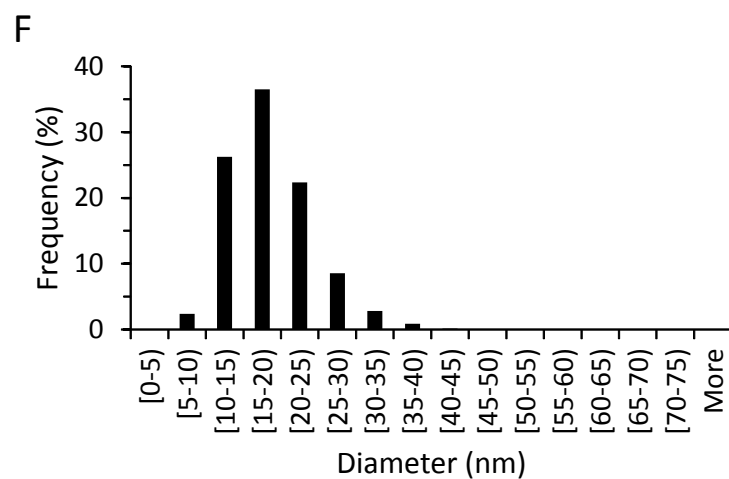
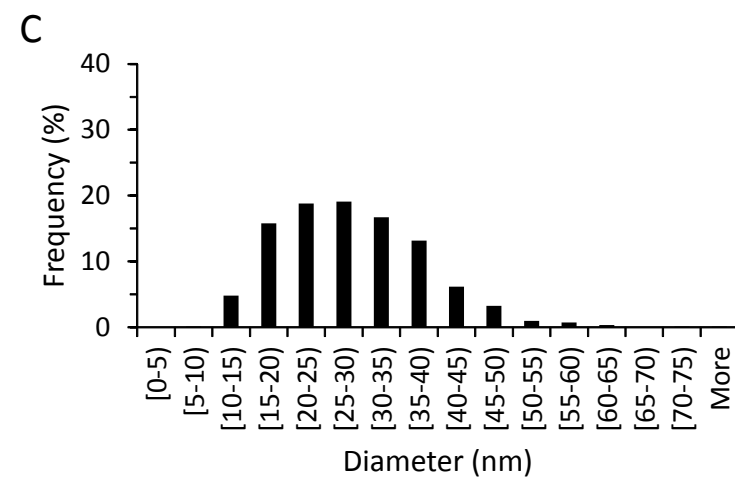
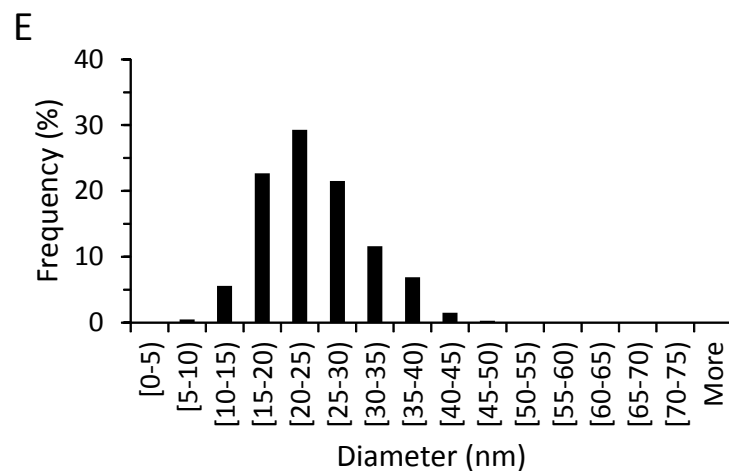
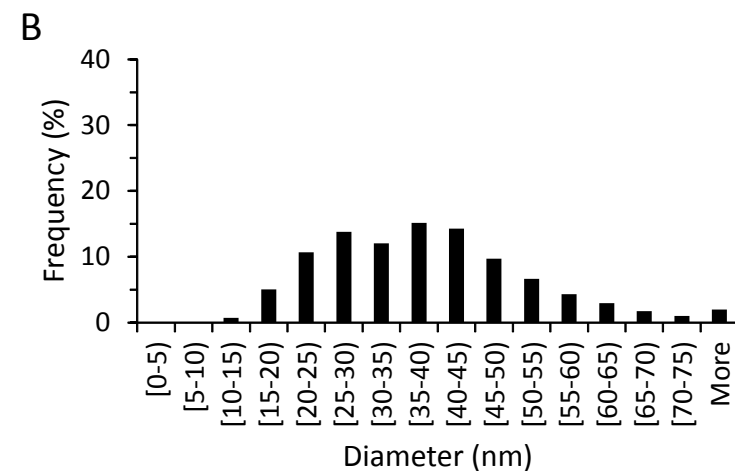
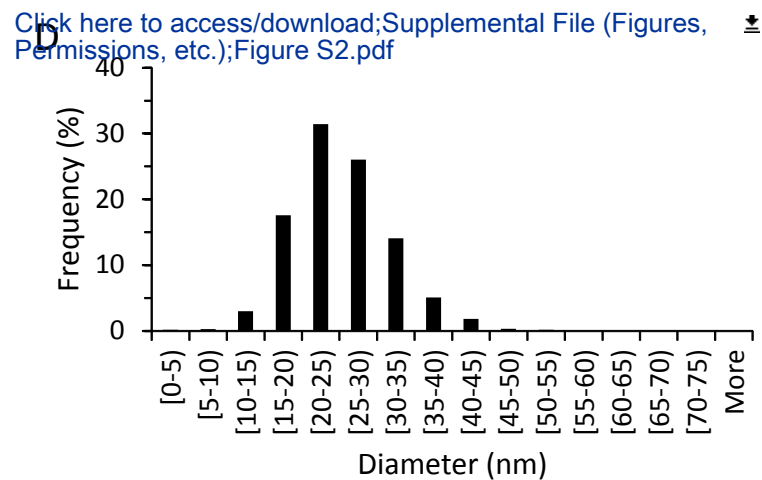
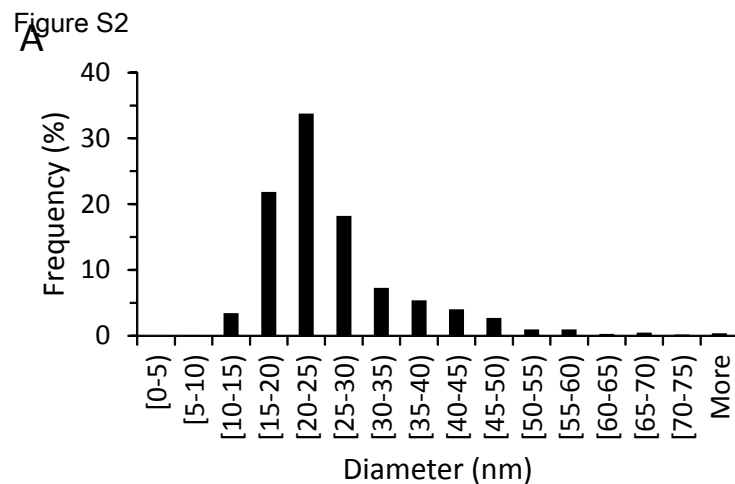
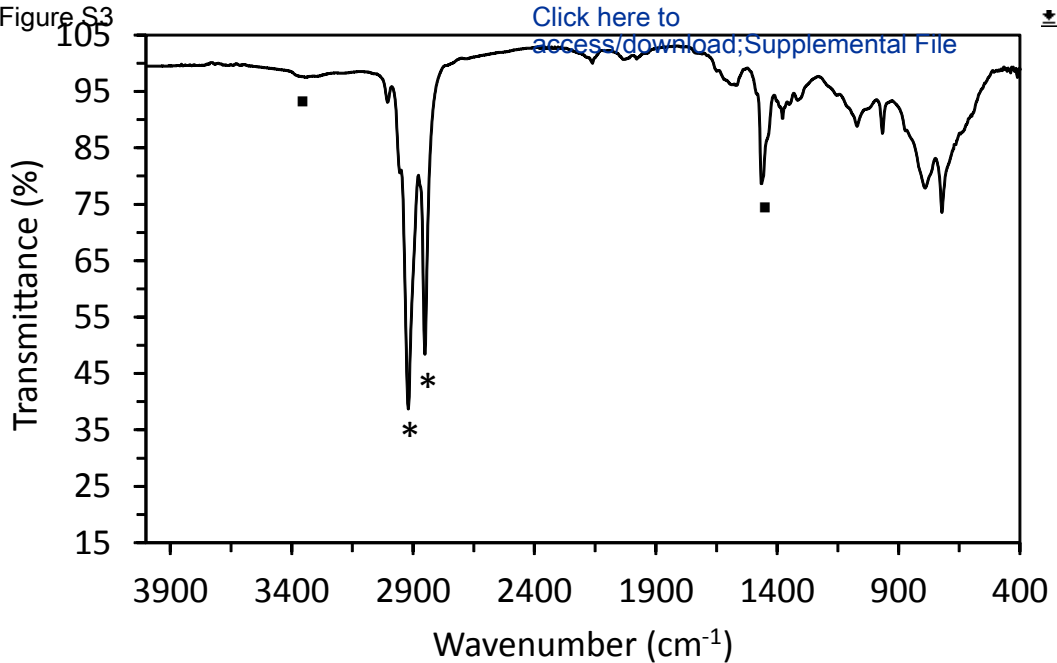




Figure S3





1 Alewife Center #200  
Cambridge, MA 02140  
tel. 617.945.9051  
www.jove.com

## ARTICLE AND VIDEO LICENSE AGREEMENT

Title of Article:	Manganese oxide nanoparticle synthesis by thermal decomposition of manganese(II) acetylacetonate
Author(s):	Celia Martinez Margaret Bennewitz

Item 1: The Author elects to have the Materials be made available (as described at <http://www.jove.com/publish>) via:



Standard Access



Open Access

Item 2: Please select one of the following items:



The Author is **NOT** a United States government employee.



The Author is a United States government employee and the Materials were prepared in the course of his or her duties as a United States government employee.

## ARTICLE AND VIDEO LICENSE AGREEMENT

1. **Defined Terms.** As used in this Article and Video License Agreement, the following terms shall have the following meanings: “**Agreement**” means this Article and Video License Agreement; “**Article**” means the article specified on the last page of this Agreement, including any associated materials such as texts, figures, tables, artwork, abstracts, or summaries contained therein; “**Author**” means the author who is a signatory to this Agreement; “**Collective Work**” means a work, such as a periodical issue, anthology or encyclopedia, in which the Materials in their entirety in unmodified form, along with a number of other contributions, constituting separate and independent works in themselves, are assembled into a collective whole; “**CRC License**” means the Creative Commons Attribution-Non Commercial-No Derivs 3.0 Unported Agreement, the terms and conditions of which can be found at: <http://creativecommons.org/licenses/by-nc-nd/3.0/legalcode>; “**Derivative Work**” means a work based upon the Materials or upon the Materials and other pre-existing works, such as a translation, musical arrangement, dramatization, fictionalization, motion picture version, sound recording, art reproduction, abridgment, condensation, or any other form in which the Materials may be recast, transformed, or adapted; “**Institution**” means the institution, listed on the last page of this Agreement, by which the Author was employed at the time of the creation of the Materials; “**JoVE**” means MyJoVE Corporation, a Massachusetts corporation and the publisher of The Journal of Visualized Experiments; “**Materials**” means the Article and / or the Video; “**Parties**” means the Author and JoVE; “**Video**” means any video(s) made by the Author, alone or in conjunction with any other parties, or by JoVE or its affiliates or agents, individually or in collaboration with the Author or any other parties, incorporating all or any portion

of the Article, and in which the Author may or may not appear.

2. **Background.** The Author, who is the author of the Article, in order to ensure the dissemination and protection of the Article, desires to have the JoVE publish the Article and create and transmit videos based on the Article. In furtherance of such goals, the Parties desire to memorialize in this Agreement the respective rights of each Party in and to the Article and the Video.

3. **Grant of Rights in Article.** In consideration of JoVE agreeing to publish the Article, the Author hereby grants to JoVE, subject to **Sections 4 and 7** below, the exclusive, royalty-free, perpetual (for the full term of copyright in the Article, including any extensions thereto) license (a) to publish, reproduce, distribute, display and store the Article in all forms, formats and media whether now known or hereafter developed (including without limitation in print, digital and electronic form) throughout the world, (b) to translate the Article into other languages, create adaptations, summaries or extracts of the Article or other Derivative Works (including, without limitation, the Video) or Collective Works based on all or any portion of the Article and exercise all of the rights set forth in (a) above in such translations, adaptations, summaries, extracts, Derivative Works or Collective Works and (c) to license others to do any or all of the above. The foregoing rights may be exercised in all media and formats, whether now known or hereafter devised, and include the right to make such modifications as are technically necessary to exercise the rights in other media and formats. If the “Open Access” box has been checked in **Item 1** above, JoVE and the Author hereby grant to the public all such rights in the Article as provided in, but subject to all limitations and requirements set forth in, the CRC License.

## ARTICLE AND VIDEO LICENSE AGREEMENT

4. **Retention of Rights in Article.** Notwithstanding the exclusive license granted to JoVE in **Section 3** above, the Author shall, with respect to the Article, retain the non-exclusive right to use all or part of the Article for the non-commercial purpose of giving lectures, presentations or teaching classes, and to post a copy of the Article on the Institution's website or the Author's personal website, in each case provided that a link to the Article on the JoVE website is provided and notice of JoVE's copyright in the Article is included. All non-copyright intellectual property rights in and to the Article, such as patent rights, shall remain with the Author.

5. **Grant of Rights in Video – Standard Access.** This **Section 5** applies if the "Standard Access" box has been checked in **Item 1** above or if no box has been checked in **Item 1** above. In consideration of JoVE agreeing to produce, display or otherwise assist with the Video, the Author hereby acknowledges and agrees that, Subject to **Section 7** below, JoVE is and shall be the sole and exclusive owner of all rights of any nature, including, without limitation, all copyrights, in and to the Video. To the extent that, by law, the Author is deemed, now or at any time in the future, to have any rights of any nature in or to the Video, the Author hereby disclaims all such rights and transfers all such rights to JoVE.

6. **Grant of Rights in Video – Open Access.** This **Section 6** applies only if the "Open Access" box has been checked in **Item 1** above. In consideration of JoVE agreeing to produce, display or otherwise assist with the Video, the Author hereby grants to JoVE, subject to **Section 7** below, the exclusive, royalty-free, perpetual (for the full term of copyright in the Article, including any extensions thereto) license (a) to publish, reproduce, distribute, display and store the Video in all forms, formats and media whether now known or hereafter developed (including without limitation in print, digital and electronic form) throughout the world, (b) to translate the Video into other languages, create adaptations, summaries or extracts of the Video or other Derivative Works or Collective Works based on all or any portion of the Video and exercise all of the rights set forth in (a) above in such translations, adaptations, summaries, extracts, Derivative Works or Collective Works and (c) to license others to do any or all of the above. The foregoing rights may be exercised in all media and formats, whether now known or hereafter devised, and include the right to make such modifications as are technically necessary to exercise the rights in other media and formats. For any Video to which this **Section 6** is applicable, JoVE and the Author hereby grant to the public all such rights in the Video as provided in, but subject to all limitations and requirements set forth in, the CRC License.

7. **Government Employees.** If the Author is a United States government employee and the Article was prepared in the course of his or her duties as a United States government employee, as indicated in **Item 2** above, and any of the licenses or grants granted by the Author hereunder exceed the scope of the 17 U.S.C. 403, then the rights granted hereunder shall be limited to the maximum

rights permitted under such statute. In such case, all provisions contained herein that are not in conflict with such statute shall remain in full force and effect, and all provisions contained herein that do so conflict shall be deemed to be amended so as to provide to JoVE the maximum rights permissible within such statute.

8. **Protection of the Work.** The Author(s) authorize JoVE to take steps in the Author(s) name and on their behalf if JoVE believes some third party could be infringing or might infringe the copyright of either the Author's Article and/or Video.

9. **Likeness, Privacy, Personality.** The Author hereby grants JoVE the right to use the Author's name, voice, likeness, picture, photograph, image, biography and performance in any way, commercial or otherwise, in connection with the Materials and the sale, promotion and distribution thereof. The Author hereby waives any and all rights he or she may have, relating to his or her appearance in the Video or otherwise relating to the Materials, under all applicable privacy, likeness, personality or similar laws.

10. **Author Warranties.** The Author represents and warrants that the Article is original, that it has not been published, that the copyright interest is owned by the Author (or, if more than one author is listed at the beginning of this Agreement, by such authors collectively) and has not been assigned, licensed, or otherwise transferred to any other party. The Author represents and warrants that the author(s) listed at the top of this Agreement are the only authors of the Materials. If more than one author is listed at the top of this Agreement and if any such author has not entered into a separate Article and Video License Agreement with JoVE relating to the Materials, the Author represents and warrants that the Author has been authorized by each of the other such authors to execute this Agreement on his or her behalf and to bind him or her with respect to the terms of this Agreement as if each of them had been a party hereto as an Author. The Author warrants that the use, reproduction, distribution, public or private performance or display, and/or modification of all or any portion of the Materials does not and will not violate, infringe and/or misappropriate the patent, trademark, intellectual property or other rights of any third party. The Author represents and warrants that it has and will continue to comply with all government, institutional and other regulations, including, without limitation all institutional, laboratory, hospital, ethical, human and animal treatment, privacy, and all other rules, regulations, laws, procedures or guidelines, applicable to the Materials, and that all research involving human and animal subjects has been approved by the Author's relevant institutional review board.

11. **JoVE Discretion.** If the Author requests the assistance of JoVE in producing the Video in the Author's facility, the Author shall ensure that the presence of JoVE employees, agents or independent contractors is in accordance with the relevant regulations of the Author's institution. If more than one author is listed at the beginning of this Agreement, JoVE may, in its sole

## ARTICLE AND VIDEO LICENSE AGREEMENT

discretion, elect not take any action with respect to the Article until such time as it has received complete, executed Article and Video License Agreements from each such author. JoVE reserves the right, in its absolute and sole discretion and without giving any reason therefore, to accept or decline any work submitted to JoVE. JoVE and its employees, agents and independent contractors shall have full, unfettered access to the facilities of the Author or of the Author's institution as necessary to make the Video, whether actually published or not. JoVE has sole discretion as to the method of making and publishing the Materials, including, without limitation, to all decisions regarding editing, lighting, filming, timing of publication, if any, length, quality, content and the like.

12. **Indemnification.** The Author agrees to indemnify JoVE and/or its successors and assigns from and against any and all claims, costs, and expenses, including attorney's fees, arising out of any breach of any warranty or other representations contained herein. The Author further agrees to indemnify and hold harmless JoVE from and against any and all claims, costs, and expenses, including attorney's fees, resulting from the breach by the Author of any representation or warranty contained herein or from allegations or instances of violation of intellectual property rights, damage to the Author's or the Author's institution's facilities, fraud, libel, defamation, research, equipment, experiments, property damage, personal injury, violations of institutional, laboratory, hospital, ethical, human and animal treatment, privacy or other rules, regulations, laws, procedures or guidelines, liabilities and other losses or damages related in any way to the submission of work to JoVE, making of videos by JoVE, or publication in JoVE or elsewhere by JoVE. The Author shall be responsible for, and shall hold JoVE harmless from, damages caused by lack of sterilization, lack of cleanliness or by contamination due to

the making of a video by JoVE its employees, agents or independent contractors. All sterilization, cleanliness or decontamination procedures shall be solely the responsibility of the Author and shall be undertaken at the Author's expense. All indemnifications provided herein shall include JoVE's attorney's fees and costs related to said losses or damages. Such indemnification and holding harmless shall include such losses or damages incurred by, or in connection with, acts or omissions of JoVE, its employees, agents or independent contractors.

13. **Fees.** To cover the cost incurred for publication, JoVE must receive payment before production and publication of the Materials. Payment is due in 21 days of invoice. Should the Materials not be published due to an editorial or production decision, these funds will be returned to the Author. Withdrawal by the Author of any submitted Materials after final peer review approval will result in a US\$1,200 fee to cover pre-production expenses incurred by JoVE. If payment is not received by the completion of filming, production and publication of the Materials will be suspended until payment is received.

14. **Transfer, Governing Law.** This Agreement may be assigned by JoVE and shall inure to the benefits of any of JoVE's successors and assignees. This Agreement shall be governed and construed by the internal laws of the Commonwealth of Massachusetts without giving effect to any conflict of law provision thereunder. This Agreement may be executed in counterparts, each of which shall be deemed an original, but all of which together shall be deemed to be one and the same agreement. A signed copy of this Agreement delivered by facsimile, e-mail or other means of electronic transmission shall be deemed to have the same legal effect as delivery of an original signed copy of this Agreement.